Power Switch Open-Circuit Fault Diagnosis of Six-Phase Fault Tolerant Permanent Magnet Synchronous Motor System Under Normal and Fault-Tolerant Operation Conditions Using the Average Current Park's Vector Approach

Hong Guo, Si Guo, Jinquan Xu, and Xinlei Tian

***Abstract*—In this article, a new power switch open-circuit fault diagnosis approach is proposed for the six-phase fault-tolerant permanent magnet synchronous motor (FTPMSM) system based on average current Park's vector (ACPV), which can detect the fault power switch for the FTPMSM system in both normal and phase open-circuit/short-circuit fault-tolerant operation conditions. To detect the power switch open-circuit fault, the fault detection approach based on the moduli of the ACPV in two orthogonal subspaces is first proposed for the six-phase FTPMSM system even in phase open-circuit and short-circuit fault-tolerant operation. Then, the ACPV-based fault location approach is proposed, which can identify the fault power switch according to the sign symbol of the ACPV. The resulting fault diagnosis approach has a simple structure and low computation burden, which can detect the power switch open-circuit fault online for the FTPMSM system in both normal and fault-tolerant operation conditions. Finally, the effectiveness of the proposed fault diagnosis approach is demonstrated by a six-phase FTPMSM system experimental platform.**

***Index Terms*—Average current Park's vector (ACPV), fault diagnosis, fault-tolerant permanent magnet synchronous motor (FTPMSM), open-circuit fault, power switch.**

I. Introduction

With the advantages of high power density, efficiency, reliability, the multiphase fault-tolerant permanent magnet synchronous motor (FTPMSM) is becoming an increasing option for aerospace application [1]–[4]. Although the FTPMSM has the fault-tolerant capability, the state that the motor operates in is abnormal when the fault occurs. If the fault cannot be diagnosed accurately and timely, it may cause further damage to the FTPMSM and even pose a serious threat to the whole system. Therefore, the fault diagnosis has become an indispensable part of the fault-tolerant control algorithm for the FTPMSM system.

There are three main sources of faults in a PMSM system, namely, motor fault, drivers fault, and sensor fault. Statistical results presented in [5] show that about 38% of failures are attributed to the power converter and the most of faults are reflected on power switch faults. In general, power switch faults can be broadly classified as short-circuit fault and open-circuit fault. The short-circuit fault is one of the most fatal accidents and it usually happens in an extremely short time. Hence, the control circuits of the power switch are often designed to prevent the abnormal overcurrent and the protection hardware circuits are usually employed. The open-circuit fault generally does not cause the system to shutdown immediately and can remain undetected for a period of time. However, it can lead to the secondary fault in the converter, resulting in the shutdown of the whole system eventually [6]. Therefore, this article concentrates on the power switch open-circuit fault that may result from physical damage or a gate driver failure.

In the past few years, several works have been presented to diagnose the open-circuit fault in motor drive systems. In general, diagnostic methods can be classified into the following three categories: model-based diagnostics, knowledge-based diagnostics, and signal based diagnostics.

Model-based methods have been widely used to detect the faults of the drive system. By employing different types of observers, such as Luenberger observer [7], [8], sliding mode observer [9], [10], nonlinear observer [11], variable structure observer [12], the methods perform effective diagnosis with relatively short detection time. In addition, the model-based method requires no extra hardware and can be insensitive to the load changes. However, since the methods are based on residual generation, the performance of the model-based method is highly dependent on the accuracy of the model and is extremely sensitive to the motor parameter variations.

Manuscript received December 11, 2019; revised March 19, 2020 and July 3, 2020; accepted August 5, 2020. Date of publication August 19, 2020; date of current version October 30, 2020. This work was supported in part by National Natural Science Foundation of China under Grant 51707004, in part by Aeronautical Science Foundation of China under Grant 201907051002, in part by the Fundamental Research Funds for the Central Universities under Grant YWF20BJJ522, in part by National Defense Science and Technology Foundation Enhancement Program, and in part by Major Program of the National Natural Science Foundation of China under Grant 51890882. Recommended by Associate Editor A. J. Marques Cardoso. *(Corresponding author: Jinquan Xu.)*

The authors are with the School of Automation Science and Electrical Engineering, Beihang University, Beijing 100000, China (e-mail: guohong_buaa@163.com; guosi@buaa.edu.cn; xujinquan@buaa.edu.cn; tianxinlei@buaa.edu.cn).

Color versions of one or more of the figures in this article are available online at https://ieeexplore.ieee.org.

Digital Object Identifier 10.1109/TPEL.2020.3017637

In previous research, the knowledge-based methods based on advanced algorithms such as expert system [13], fuzzy logic [14], [15], neural network [16], echo state network [17], and deep learning technology [18] have also been proposed for power switch fault diagnostic. Since the knowledge-based method is basing on the system historic data, it does not require an accurate system model. However, this method needs a long training time and a huge computational effort, which greatly increase the realization difficulty. Therefore, the knowledge-based method is hard to be integrated into the drive controller and too complex for real-time implementation.

The signal-based method is realized by extracting specific features of the faulty signals. According to the measured variables, the methods can be classified into voltage-based and current-based method. As to voltage-based method, the diagnostic is able to detect the fault very fast. As presented in [19]–[22], the detection time can be less than 10 μs. However, the methods usually need extra voltage sensors, which increase the system cost, complexity, and potential fault points. The fault diagnostic methods based on the current signal have also been extensively addressed in the literature. Since the current-based method is closely related to the fundamental current period, the fault diagnostic time is commonly longer than voltage-based methods. The major advantage of the current-based method is that there is no dependence on system parameters and no requirement of additional hardware. Different schemes employing tools such as slope method, Park's vector method, and dc method have been presented to obtain an effective fault detection index [23], [24]. The current Park's vector approach was proposed in [25] as a diagnostic tool for inverter faults. Since this approach requires complex pattern recognition algorithms, it's difficult to integrate into the drive controller. Much later proposed fault diagnosis methods are based on this approach. The average current Park's vector (ACPV) approach was introduced for diagnosing voltage source inverter faults in variable speed ac drives in [26], which relies on inspection of the average motor current Park's Vector modulus and phase. In order to reduce the possibility of misinterpreting a transient regime, the detection is made using both the modulus and the angle of the ACPV in [27]. A fault diagnostic approach based on the derivative of the absolute current Park's vector was introduced in [28]. The open-circuit faults are detected by determining whether the detection variable reaches the threshold and the faulty switch is localized through the polarity and the values of the current. In [29], the errors of the normalized currents' average absolute values are taken as diagnostic variables that allow for the detection of single and multiple open-circuit faults. However, the approach's robustness against speed variation is not considered. In [30] and [31], the fault symptom variables of the motor drives are calculated by using the ACPV method and then processed by a fuzzy logic approach. However, all the aforementioned methods are used to detect the open-circuit fault of the conventional three-phase motor drives, which is based on a single $\alpha\beta$ subspace and not suitable for the open-circuit fault diagnosis of the multiphase FTPMSM.

The literature review shows that, despite all the existing work concerning the diagnostic method for open-circuit faults in power converters, there is still rare research work on detection and identification of open-circuit fault in multiphase FTPMSM. In [32], a centroid-based diagnostic method for power switches in a five-phase PMSM inverter is proposed. By using multiple normalized variables derived from the normalized phase current, this approach offers a simple diagnostic process of switch fault regardless of the transient states. In [33], a comprehensive diagnostic method for electrical faults and sensor faults in dual three-phase PMSM drives is proposed, which can identify open-switch fault and current sensor fault simultaneously. However, all these diagnostic methods are applied for fault diagnosis under normal operation condition and no solution was offered for the secondary power switch open-circuit fault diagnosis in FTPMSM under fault-tolerant operation condition.

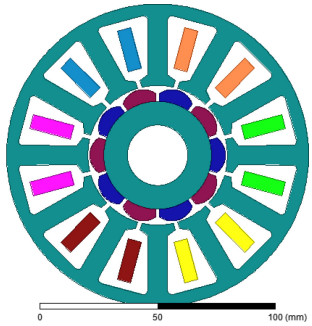

Fig. 1. Structure of one segment of the six-phase FTPMSM.

Therefore, the objective of this article is to further explore power switch open-circuit fault diagnosis for the FTPMSM system under both normal and phase open-circuit/short-circuit fault-tolerant operation conditions. This was not available earlier and the problem is extremely important for the FTPMSM system. The main contributions of this article are fourfold. First, the fault diagnostic method is proposed to detect the power switch open-circuit fault based on the moduli of the ACPV in two orthogonal subspaces. Second, the fault location approach is proposed to identify the faulty switch according to the sign symbol of the ACPV. Third, due to the simple structure of the method, the algorithm can be readily integrated into the fault-tolerant control system, which requires no extra current or voltage sensors. Finally, the simulation and experiment are carried out to validate the proposed approach. The results show a reliable and speedy performance of the diagnostic method in both normal and open-circuit/short-circuit fault-tolerant conditions. This article innovatively employs a power switch open-circuit fault diagnostic approach that lays the foundation for the continuous operation of the FTPMSM system with multiple fault conditions.

II. Six-Phase FTPMSM System

A. Six-Phase FTPMSM

In order to enhance the fault-tolerant capacity, the six-phase FTPMSM is adopted with the alternate-teeth-wound fractional-slot concentrated windings, as shown in Fig. 1, which has the

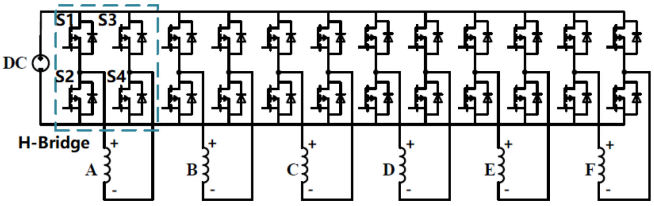

Fig. 2. H-bridge inverter structure of the six-phase FTPMSM.

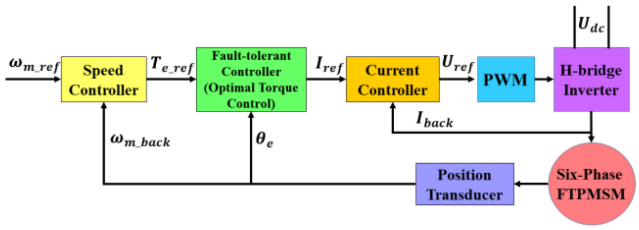

Fig. 3. Dual closed-loop control structure of the six-phase FTPMSM.

advantages of magnetic isolation and physical isolation. Furthermore, the motor has a relatively small mutual inductance that can reduce the effect of the faulty phase winding on normal phases when the fault occurs. In addition, the slot dimension is designed to increase the phase self-inductance, which can prevent the excessive short-circuit current.

B. Inverter System

In order to realize the electric isolation capacity among the phase windings of the FTPMSM, the H-bridge based inverter is adopted in this article, which is shown in Fig. 2. This structure can supply the power for each phase winding independently, which can avoid electrical interference of the faulty phase winding to the normal phase windings.

C. Fault-Tolerant Control Strategy

In order to reduce torque ripple under the open-circuit and short-circuit fault conditions, the optimal torque control is adopted in this article.

The optimal torque control aims at achieving a ripple-free electromagnetic torque under both normal and faulted conditions with minimum stator copper loss [34]. The electromagnetic torque of a normal six-phase FTPMSM can be written as

$$T_e = \sum_{i \in S} k_i I_i \ , \ \{S \in \{a, b, \ c, \ d, \ e, \ f\}\} \tag{1}$$

with

$$k_i = k_m \sin(\omega_e t + \theta_{ei}), \left\{\theta_{ei} \in \left\{0, \ \frac{\pi}{3}, \ \frac{2\pi}{3}, \ \pi, \ \frac{4\pi}{3}, \ \frac{5\pi}{3}\right\}\right\}. \tag{2}$$

When the FTPMSM is under fault condition, the electromagnetic torque can be written as

$$T_e = \sum_{i \in S_N} k_i I_i + \sum_{j \in S_F} k_j I_j = T_N + T_F \tag{3}$$

with

$$T_F = \begin{cases} 0, \ \text{for an open} - \text{circuit fault} \\ k_j I_j, \ \text{for a short} - \text{circuit fault} \end{cases} \tag{4}$$

where T_e denotes the electromagnetic torque, S is the set of the phase windings, K_i denotes the instantaneous ratio of the phase electromotive force (EMF) to the rotor speed, I_i is the phase current, K_m denotes the peak EMF coefficient, ω_e denotes the electrical angular speed, θ_e denotes the electrical angular position, S_N denotes the set of the normal phase windings, S_F denotes the set of the fault phase windings, T_N denotes the instantaneous torque developed by the normal phase, and T_F denotes the instantaneous torque developed by the fault phase.

The constrained optimization problem of copper loss can be represented as

$$\min R \sum_{i \in S_N} I_i^2 \tag{5}$$

where R is the phase winding resistance.

By Lagrange multiplier method, the instantaneous phase currents in the remaining healthy phases are given by

$$I_j = \frac{(T_e - T_F)\, k_m \sin(\omega_e t + \theta_{ej})}{\sum_{i \in S_N} k_m^2 \sin^2(\omega_e t + \theta_{ei})}. \tag{6}$$

The dual closed-loop control structure of the six-phase FTPMSM is shown in Fig. 3. Note that the outer loop is a speed loop and the inner loop is an optimal torque control based current loop. The optimal torque control is an instantaneous torque control strategy. According to the reference torque generated by speed controller, electrical angular position, and the instantaneous torque developed by the fault phase, the current references are then calculated by the fault-tolerant controller based on (6). In fault-tolerant operation condition, the remaining healthy phase currents of the FTPMSM are taken in the form of (6) to generate the smooth electromagnetic torque, regardless of phase open-circuit and short-circuit faults.

III. Proposed Fault Diagnosis Method

In this section, we propose the ACPV-based fault diagnosis method for the power switch open-circuit fault of the six-phase FTPMSM system under both the normal and phase open-circuit/short-circuit fault-tolerant operation conditions, which was not available earlier. The essence of the proposed fault diagnosis is to achieve the detection of power switch open-circuit fault and the localization of the faulty switch by the values of the ACPV of the phase currents.

In the conventional three-phase motor system, the ACPV approach is based on a single $\alpha\beta$ subspace. In order to obtain more information and achieve a high robustness against transients, two orthogonal subspaces are employed in the proposed ACPV approach. The phase currents of the six-phase FTPMSM can be

transformed as

$$\begin{bmatrix} I_{\alpha 1} \\ I_{\beta 1} \\ I_{\alpha 2} \\ I_{\beta 2} \end{bmatrix} = \frac{1}{\sqrt{3}} [C] \begin{bmatrix} I_a \\ I_b \\ I_c \\ I_d \\ I_e \\ I_f \end{bmatrix} \tag{7}$$

with

$$[C] = \begin{bmatrix} 1 & \cos\left(\frac{\pi}{3}\right) & -1 & \cos\left(\frac{4\pi}{3}\right) & \cos\left(\frac{5\pi}{3}\right) \\ 0 & \sin\left(\frac{\pi}{3}\right) & 0 & \sin\left(\frac{4\pi}{3}\right) & \sin\left(\frac{5\pi}{3}\right) \\ 1 & \cos\left(\frac{2\pi}{3}\right) & 1 & \cos\left(\frac{8\pi}{3}\right) & \cos\left(\frac{10\pi}{3}\right) \\ 0 & \sin\left(\frac{2\pi}{3}\right) & 0 & \sin\left(\frac{8\pi}{3}\right) & \sin\left(\frac{10\pi}{3}\right) \end{bmatrix} \tag{8}$$

where I_a, I_b, I_c, I_d, I_e, and I_f are the phase currents, $(I_{\alpha 1},\ I_{\beta 1})$and $(I_{\alpha 2},\ I_{\beta 2})$ are the current Park's vector components which belongs to the orthogonal subspaces $S_{\alpha_1\beta_1}$ and $S_{\alpha_2\beta_2}$, respectively. Under the normal condition, the current vector in first two-dimensional subspace $S_{\alpha_1\beta_1}$ generates the rotating magnetomotive force, which is the origin of the most part of torque. Meanwhile, in subspace $S_{\alpha_2\beta_2}$, the space vectors composed of phase A, C, E and phase B, D, F have the same magnitude but opposite directions, and therefore, the resultant current vector is equal to zero under normal condition. As a consequence, the vector in subspace $S_{\alpha_2\beta_2}$ should be robust to transients of currents during speed and load torque change. The current Park's vector components can be expressed by

$$\begin{aligned} I_1 &= I_{\alpha 1} + j \cdot I_{\beta 1} = I_{\mathrm{mod}1} \angle \theta_1 \\ I_2 &= I_{\alpha 2} + j \cdot I_{\beta 2} = I_{\mathrm{mod}2} \angle \theta_2 \end{aligned} \tag{9}$$

where

$$\begin{aligned} I_{\alpha 1} &= \tfrac{1}{\sqrt{3}} \left(I_a + \tfrac{1}{2} I_b - \tfrac{1}{2} I_c - I_d - \tfrac{1}{2} I_e + \tfrac{1}{2} I_f\right) \\ I_{\beta 1} &= \tfrac{1}{2} \left(I_b + I_c - I_e - I_f\right) \\ \theta_1 &= \tan^{-1}\left(I_{\beta 1}/I_{\alpha 1}\right) \\ I_{\alpha 2} &= \tfrac{1}{\sqrt{3}} \left(I_a - \tfrac{1}{2} I_b - \tfrac{1}{2} I_c + I_d - \tfrac{1}{2} I_e - \tfrac{1}{2} I_f\right) \\ I_{\beta 2} &= \tfrac{1}{2} \left(I_b - I_c + I_e - I_f\right) \\ \theta_2 &= \tan^{-1}\left(I_{\beta 2}/I_{\alpha 2}\right). \end{aligned} \tag{10}$$

Therefore, the average values of the current Park's vector over one period can be calculated by

$$\begin{aligned} I_{\alpha 1_{\mathrm{av}}} &= \frac{1}{T} \int_0^T I_{\alpha 1} dt \\ I_{\beta 1_{\mathrm{av}}} &= \frac{1}{T} \int_0^T I_{\beta 1} dt \\ I_{\mathrm{mod}1} &= \sqrt{I_{\alpha 1_{\mathrm{av}}}^2 + I_{\beta 1_{\mathrm{av}}}^2} \\ \theta_1 &= \tan^{-1}\left(I_{\beta 1_{\mathrm{av}}}/I_{\alpha 1_{\mathrm{av}}}\right) \\ I_{\alpha 2_{\mathrm{av}}} &= \frac{1}{T} \int_0^T I_{\alpha 2} dt \\ I_{\beta 2_{\mathrm{av}}} &= \frac{1}{T} \int_0^T I_{\beta 2} dt \\ I_{\mathrm{mod}2} &= \sqrt{I_{\alpha 2_{\mathrm{av}}}^2 + I_{\beta 2_{\mathrm{av}}}^2} \\ \theta_2 &= \tan^{-1}\left(I_{\beta 2_{\mathrm{av}}}/I_{\alpha 2_{\mathrm{av}}}\right) \end{aligned} \tag{11}$$

where $I_{\alpha 1_{\mathrm{av}}}$, $I_{\beta 1_{\mathrm{av}}}$, $I_{\alpha 2_{\mathrm{av}}}$, and $I_{\beta 2_{\mathrm{av}}}$ are the average value of the *d* and *q* components of the current Park's vector, $I_{\mathrm{mod}1}$ and $I_{\mathrm{mod}2}$ are the moduli of the current Park's vector, θ_1 and θ_2 are the current Park's vector angles, and T is the fundamental current period.

To achieve the fault diagnosis for the six-phase FTPMSM system under the normal and phase open-circuit/short-circuit fault-tolerant operation conditions, the values of the ACPV before and after the power switch open-circuit fault will be thoroughly analyzed in the following.

A. Values of ACPV Before Power Switch Open-Circuit Fault

1) Normal Operation Condition: Under the normal operation condition, according to the optimal torque control algorithm, the instantaneous phase current command in each phase can be represented as

$$\begin{aligned} I_i &= \frac{T_g \times k_m \sin\left(\omega_e t + \theta_i\right)}{K_{\mathrm{SUM}}} \\ \theta_i &\in \left\{0, \frac{\pi}{3}, \cdots, \frac{5\pi}{3}\right\},\ \{i \epsilon \{a, b, c, d, e, f\}\} \end{aligned} \tag{12}$$

with

$$\begin{aligned} K_{\mathrm{SUM}} = k_m^2 \Bigg(& \sin^2\left(\omega_e t\right) + \sin^2\left(\omega_e t + \frac{\pi}{3}\right) \\ & + \sin^2\left(\omega_e t + \frac{2\pi}{3}\right) + \sin^2\left(\omega_e t + \pi\right) \\ & + \sin^2\left(\omega_e t + \frac{4\pi}{3}\right) + \sin^2\left(\omega_e t + \frac{5\pi}{3}\right)\Bigg) \\ = 3k_m^2 \end{aligned} \tag{13}$$

where T_g is the reference torque given by speed controller and θ_i is the phase angle.

Then the average value of each phase current over one period is zero

$$\begin{aligned} I_{i_{av}} &= \frac{1}{T} \int_0^T I_i dt \\ &= \frac{1}{T} \cdot \frac{T_g}{3k_m} \int_0^T \sin\left(\omega_e t + \theta_i\right) dt \\ &= 0, \{\ i \epsilon \{a, b, c, d, e, f\}\}. \end{aligned} \tag{14}$$

Therefore, the moduli of the ACPV are zero as well

$$\begin{aligned} I_{\alpha 1_{\mathrm{av}}} &= I_{\beta 1_{\mathrm{av}}} = I_{\alpha 2_{\mathrm{av}}} = I_{\beta 2_{\mathrm{av}}} = 0 \\ I_{\mathrm{mod}1} &= I_{\mathrm{mod}2} = 0. \end{aligned} \tag{15}$$

2) Single Phase Open-Circuit Fault-Tolerant Operation Condition: Under the single-phase open-circuit fault-tolerant operation condition, the faulty phase current is zero

$$I_j = 0,\ \{j \in S_F\}. \tag{16}$$

By (6), the phase currents in the remaining healthy phases are nonsinusoidal. The integral of the nonfault phase current over

one period can be represented as

$$\int_0^T I_i dt = \int_0^T \frac{T_g \times k_m \sin(\omega_e t + \theta_i)}{K_{\mathrm{SUM1}}} dt, \ \{i \in S_N\} \quad (17)$$

with

$$K_{\mathrm{SUM1}} = k_m^2 \left(3 - \sin^2(\omega_e t + \theta_j)\right), \{ j \in S_F\}. \quad (18)$$

Theorem 1: Under single-phase open-circuit fault-tolerant operation, the moduli of the ACPV are zero.

Proof: We prove this by computing definite integrals of each phase current over one fundamental current period. By (17), define the function $f(x)$ as

$$f(x) = \frac{T_g \times k_m \sin(x + \theta_i)}{k_m^2 (3 - \sin^2(x + \theta_j))}, \{ i \in S_N;\ j \in S_F\} \quad (19)$$

with

$$\begin{aligned} x &= \omega_e t \\ T &= 2\pi/\omega_e. \end{aligned} \quad (20)$$

The periodicity of the function $f(x)$ can be represented as

$$\begin{aligned} f(x + 2\pi) &= \frac{T_g \times k_m \sin(x + \theta_i + 2\pi)}{k_m^2 (3 - \sin^2(x + \theta_j + 2\pi))} \\ &= \frac{T_g \times k_m \sin(x + \theta_i)}{k_m^2 (3 - \sin^2(x + \theta_j))} = f(x). \end{aligned} \quad (21)$$

The odevity of the function $f(x)$ can be represented as

$$\begin{aligned} f(x + \pi) &= \frac{T_g \times k_m \sin(x + \theta_i + \pi)}{k_m^2 (3 - \sin^2(x + \theta_j + \pi))} \\ &= -\frac{T_g \times k_m \sin(x + \theta_i)}{k_m^2 (3 - \sin^2(x + \theta_j))} = -f(x). \end{aligned} \quad (22)$$

With (21) and (22), the integral of the nonfault phase current over one period can be obtained as

$$\begin{aligned} \int_0^{2\pi} f(x)\, dx &= \int_0^{\pi} f(x)\, dx + \int_{\pi}^{2\pi} f(x)\, dx \\ &= \int_0^{\pi} f(x)\, dx + \int_0^{\pi} f(y + \pi)\, dy \\ &= \int_0^{\pi} f(x)\, dx - \int_0^{\pi} f(y)\, dy \\ &= 0. \end{aligned} \quad (23)$$

By (17) and (23), the average value of the nonfault phase current over one period can be calculated by

$$I_{i_{av}} = \frac{1}{T} \int_0^T I_i dt = 0, \ \{i \in S_N\}. \quad (24)$$

Hence, the moduli of the ACPV are proved to be zero

$$\begin{aligned} &I_{\alpha 1_{\mathrm{av}}} = I_{\beta 1_{\mathrm{av}}} = I_{\alpha 2_{\mathrm{av}}} = I_{\beta 2_{\mathrm{av}}} = 0 \\ &I_{\mathrm{mod1}} = I_{\mathrm{mod2}} = 0. \end{aligned} \quad (25)$$

3) Single-Phase Short-Circuit Fault-Tolerant Operation Condition: Under the single-phase short-circuit fault-tolerant operation condition, the fault phase current can be represented as

$$I_{sj} = -I_{sm} \sin\left(\omega_e t + \theta_j - \frac{\pi}{2}\right), \{ j \in S_F\} \quad (26)$$

where I_{sm} is the amplitude of the short-circuit current.

Note that the mean value of the short-circuit current over one period is zero

$$I_{sj_{\mathrm{av}}} = -\frac{1}{T} I_{sm} \int_0^T \sin\left(\omega_e t + \theta_j - \frac{\pi}{2}\right) dt = 0. \quad (27)$$

By (6), the integral of the residual nonfault phase current over one period can be represented as

$$\begin{aligned} \int_0^T I_i dt &= \int_0^T \frac{(T_g - k_m \sin 2(\omega_e t + \theta_j)) \times k_m \sin(\omega_e t + \theta_i)}{K_{\mathrm{SUM1}}} dt \\ &= \int_0^T \frac{(T_g - k_m \sin 2(\omega_e t + \theta_j)) \times k_m \sin(\omega_e t + \theta_i)}{k_m^2 (3 - \sin^2(x + \theta_j))} dt \\ &\{i \in S_N; j \in S_F\}. \end{aligned} \quad (28)$$

Theorem 2: Under single-phase short-circuit fault-tolerant operation condition, the moduli of the ACPV are zero.

Proof: We prove this by computing definite integrals of each phase current over one period. By (28), define the function $g(x)$ as

$$g(x) = \frac{(T_g - k_m \sin 2(\omega_e t + \theta_j)) \times k_m \sin(\omega_e t + \theta_i)}{k_m^2 (3 - \sin^2(x + \theta_j))}. \quad (29)$$

The periodicity of the function $g(x)$ can be represented as

$$\begin{aligned} g(x + 2\pi) &= \frac{(T_g - k_m \sin 2(\omega_e t + \theta_j + 2\pi)) \times k_m \sin(\omega_e t + \theta_i + 2\pi)}{k_m^2 (3 - \sin^2(x + \theta_j + 2\pi))} \\ &= \frac{(T_g - k_m \sin 2(\omega_e t + \theta_j)) \times k_m \sin(\omega_e t + \theta_i)}{k_m^2 (3 - \sin^2(x + \theta_j))} \\ &= g(x). \end{aligned} \quad (30)$$

The odevity of the function $g(x)$ can be represented as

$$\begin{aligned} g(x + \pi) &= \frac{(T_g - k_m \sin 2(\omega_e t + \theta_j + \pi)) \times k_m \sin(\omega_e t + \theta_i + \pi)}{k_m^2 (3 - \sin^2(x + \theta_j + \pi))} \\ &= \frac{(T_g - k_m \sin 2(\omega_e t + \theta_j)) \times (-k_m \sin(\omega_e t + \theta_i))}{k_m^2 (3 - \sin^2(x + \theta_j))} \\ &= -g(x). \end{aligned} \quad (31)$$

By (30) and (31), the integral of the nonfault phase current over one period can be obtained as

$$\begin{aligned} \int_0^{2\pi} g(x)\, dx &= \int_0^{\pi} g(x)\, dx + \int_{\pi}^{2\pi} g(x)\, dx \\ &= \int_0^{\pi} g(x)\, dx + \int_0^{\pi} g(y + \pi)\, dy \\ &= \int_0^{\pi} g(x)\, dx - \int_0^{\pi} g(y)\, dy \\ &= 0. \end{aligned} \quad (32)$$

Hence, by (28) and (32), the average value of the nonfault phase current over one period can be calculated by

$$I_{i_{\mathrm{av}}} = \frac{1}{T} \int_0^T I_i dt = 0, \ \{i \in S_N\}. \quad (33)$$

The moduli of the ACPV are proved to be zero

$$\begin{aligned} &I_{\alpha 1_{\mathrm{av}}} = I_{\beta 1_{\mathrm{av}}} = I_{\alpha 2_{\mathrm{av}}} = I_{\beta 2_{\mathrm{av}}} = 0 \\ &I_{\mathrm{mod1}} = I_{\mathrm{mod2}} = 0. \end{aligned} \quad (34)$$

Therefore, according to the Theorems 1 and 2, the moduli of the ACPV remain at zero not only under the normal operation conditio, but also under the single-phase open-circuit and short-circuit fault-tolerant operation conditions.

B. Values of ACPV After Power Switch Open-Circuit Fault

1) Single Power Switch Open-Circuit Fault Under Normal Operation Condition: After the single power switch open-circuit fault occurs, the instantaneous phase current command in each phase remains sinusoidal. Therefore, the average values of the nonfault phase currents over one period are almost zero.

Meanwhile, a half period of the phase current in the faulty phase will become zero. Due to the open-circuit fault, the speed of the FTPMSM will be affected. Therefore, the reference torque given by the speed controller will change correspondingly. Then the definite integrals of faulty phase current over one period can be represented as

$$\int_0^T I_i dt = \begin{cases} \displaystyle\int_{T/2}^{T} \frac{T_g' \times k_m \sin(\omega_e t + \theta_i)}{3k_m^2} dt, \ S_1 \text{ or } S_4 \text{ fault} \\ \displaystyle\int_{0}^{T/2} \frac{T_g' \times k_m \sin(\omega_e t + \theta_i)}{3k_m^2} dt, \ S_2 \text{ or } S_3 \text{ fault} \end{cases} \{i \in S_F\}. \tag{35}$$

According to the symmetry of the integrand, we assume that

$$\int_0^T I_i dt = \begin{cases} -m_1 < 0, \ S_1 \text{ or } S_4 \text{ fault} \\ m_1 > 0, \ S_2 \text{ or } S_3 \text{ fault.} \end{cases} \tag{36}$$

Therefore, by (11), all the values of the ACPV can be calculated. The power switch open-circuit fault in S1 or S4 of phase-A is taken as an example only for demonstration purpose. We have

$$\begin{aligned} I_{b_{\rm av}} &= I_{c_{\rm av}} = I_{d_{\rm av}} = I_{e_{\rm av}} = I_{f_{\rm av}} = 0 \\ I_{a_{\rm av}} &= \frac{1}{T} \cdot (-m_1) < 0 \\ I_{\alpha 1_{\rm av}} &= \frac{-1}{T\sqrt{3}} m_1 < 0 \\ I_{\beta 1_{\rm av}} &= 0 \\ I_{\rm mod1} &= \sqrt{I_{\alpha 1_{\rm av}}^2 + I_{\beta 1_{\rm av}}^2} = \frac{1}{T\sqrt{3}} m_1 \\ I_{\alpha 2_{\rm av}} &= \frac{1}{T\sqrt{3}} m_1 > 0 \\ I_{\beta 2_{\rm av}} &= 0 \\ I_{\rm mod2} &= \sqrt{I_{\alpha 2_{\rm av}}^2 + I_{\beta 2_{\rm av}}^2} = \frac{1}{T\sqrt{3}} m_1. \end{aligned} \tag{37}$$

Likewise, we can calculate the values of the ACPV in other power switch open-circuit fault situations under the normal operation condition. According to the calculation results under each conditions, after the single power switch open-circuit fault occurrence, the module of ACPV in subspace $S_{\alpha_1\beta_1}$ is same as the subspace $S_{\alpha_2\beta_2}$ and both will be greater than zero. Therefore, the moduli of ACPV in two orthogonal subspaces are used to detect the power switch open-circuit fault. Since there exist twelve situations of single power switch open-circuit fault under normal condition in all, we take the value of $I_{\alpha 1\_\rm av}$, $I_{\beta 1\_\rm av}$, $I_{\alpha 2\_\rm av}$, and $I_{\beta 2\_\rm av}$ as fault location variables. Therefore, the relationship between the faulty switch and the value of fault location variables can be shown in Table I.

TABLE I
LOOK-UP TABLE FOR SINGLE POWER SWITCH OPEN-CIRCUIT FAULT IDENTIFICATION UNDER NORMAL OPERATION CONDITION

Fault Switch	$I_{\alpha 1_{av}}$	Flag A1	$I_{\beta 1_{av}}$	Flag B1	$I_{\alpha 2_{av}}$	Flag A2	$I_{\beta 2_{av}}$	Flag B2
A_S1/S4	<0	0	0	1	<0	0	0	1
A_S2/S3	>0	2	0	1	>0	2	0	1
B_S1/S4	<0	0	<0	0	>0	2	<0	0
B_S2/S3	>0	2	>0	2	<0	0	>0	2
C_S1/S4	>0	2	<0	0	>0	2	>0	2
C_S2/S3	<0	0	>0	2	<0	0	<0	0
D_S1/S4	>0	2	0	1	<0	0	0	1
D_S2/S3	<0	0	0	1	>0	2	0	1
E_S1/S4	>0	2	>0	2	>0	2	<0	0
E_S2/S3	<0	0	<0	0	<0	0	>0	2
F_S1/S4	<0	0	>0	2	>0	2	>0	2
F_S2/S3	>0	2	<0	0	<0	0	<0	0

2) Single Power Switch Open-Circuit Fault under Single-Phase Open-Circuit Fault-Tolerant Operation Condition

During one phase open-circuit fault-tolerant operation, the optimal torque control is adopted to guarantee the smooth electromagnetic torque generation, in which the nonfault phase currents are nonsinusoidal, which can be given as

$$I_i = \frac{T_g'' \times k_m \sin(\omega_e t + \theta_i)}{k_m^2 (3 - \sin^2(\omega_e t + \theta_j))}, \ \{i \in S_N; \ j \in S_{F1}\} \tag{38}$$

When the power switch open-circuit fault occurs in this situation, the nonfault phase current waveforms remain unchanged, while the amplitude value T_g'' may increase due to the regulation of the speed controller. According to Theorem 1, the integral of the nonfault phase current over one period is zero.

Meanwhile, the half period of the phase current in the secondary fault phase will become zero. Then the definite integral of the secondary fault phase current over one period can be represented as

$$\begin{aligned} \int_0^T I_k &= \begin{cases} \displaystyle\int_0^T I_k dt \\ \displaystyle\int_{T/2}^{T} \frac{T_g'' \times k_m \sin(\omega_e t + \theta_k)}{k_m^2 \left(3 - \sin^2(\omega_e t + \theta_j)\right)} dt, \ S_1 \text{ or } S_4 \text{ fault} \\ \displaystyle\int_{0}^{T/2} \frac{T''_g \times k_m \sin(\omega_e t + \theta_k)}{k_m^2 (3 - \sin^2(\omega_e t + \theta_j))} dt, \ S_2 \text{ or } S_3 \text{ fault} \end{cases} \\ &\{ j \in S_{F1}; \ k \in S_{F2} \}. \end{aligned} \tag{39}$$

We assume that

$$\int_0^T I_k dt = \begin{cases} -m_2 < 0, \ S_1 \text{ or } S_4 \text{ fault} \\ m_2 > 0, \ S_2 \text{ or } S_3 \text{ fault} \end{cases} \tag{40}$$

where S_{F1} denotes the set of the primary open-circuit fault phase winding and S_{F2} denotes the set of the secondary open-circuit fault phase winding.

In the same way, we can calculate the values of ACPV of all the situations under the single-phase open-circuit fault-tolerant operation. The relationship between the faulty power switch

and the value of fault location variables are the same as the relationship in Table I.

3) Single Power Switch Open-Circuit Fault Under Single Phase Short-Circuit Fault-Tolerant Operation Condition: When the power switch open-circuit fault occurs in one-phase short-circuit fault-tolerant operation condition, by (6), the remaining nonfault phase current can be represented as

$$I_i = \frac{\left(T_g''' - k_m \sin 2\left(\omega_e t + \theta_j\right)\right) \times k_m \sin\left(\omega_e t + \theta_i\right)}{k_m^2\left(3 - \sin^2\left(x + \theta_j\right)\right)} \quad \{i \in S_N;\ j \in S_{F1}\}. \tag{41}$$

By (41) and Theorem 2, the integrals of the nonfault phase current and the short-circuit current over one period are both almost zero

$$\int_0^T I_{sj} dt = \int_0^T I_i dt \ = \ 0. \tag{42}$$

The definite integral of the secondary fault phase current over one period can be represented as

$$\int_0^T I_k dt (43) = \begin{cases} \int_{T/2}^{T} \frac{\left(T_g''' - k_m \sin 2(\omega_e t + \theta_j)\right) \times k_m \sin(\omega_e t + \theta_i)}{k_m^2 (3 - \sin^2(x + \theta_j))}\, dt \\ \qquad S_1 \text{ or } S_4 \text{ fault} \\ \int_0^{T/2} \frac{\left(T_g''' - k_m \sin 2(\omega_e t + \theta_j)\right) \times k_m \sin(\omega_e t + \theta_i)}{k_m^2 (3 - \sin^2(x + \theta_j))}\, dt, \\ \qquad S_2 \text{ or } S_3 \text{ fault} \end{cases} \quad \{\, j \in S_{F1};\ k \in S_{F2}\}. \tag{43}$$

Assume that

$$\int_0^T I_k dt = \begin{cases} -m_3 < 0, & S_1 \text{ or } S_4 \text{ fault} \\ m_3 > 0, & S_2 \text{ or } S_3 \text{ fault} \end{cases} \tag{44}$$

Then the values of ACPV in all situations under the single-phase short-circuit fault-tolerant operation can be calculated. Note that the fault diagnosis variables in one-phase short-circuit fault-tolerant operation condition are consistent with that in the normal operation condition as well, as shown in Table I.

Therefore, the proposed ACPV-based fault diagnosis approach can accurately locate the fault power switch by the values of the ACPV for the six-phase FTPMSM system under both normal and one-phase open-circuit/short-circuit fault-tolerant operation conditions, which lays the foundation for the multiple fault-tolerant operation of the FTPMSM system.

By (6) and (11), after the single-power switch open-circuit fault occurrence, the moduli of the ACPV can be represented as

$$\begin{aligned} I_{\mathrm{mod1}} &= I_{\mathrm{mod2}} \\ &= \frac{1}{\sqrt{3}} \times \frac{1}{T} \left| \int_0^T I_j dt \right| \\ &= \begin{cases} \frac{1}{T\sqrt{3}} \left| \int_{T/2}^{T} \frac{(T_e - T_F) k_m \sin(\omega_e t + \theta_{ej})}{\sum_{i \in S_N} k_m^2 \sin^2(\omega_e t + \theta_{ei})} dt \right|, & S_1 \text{ or } S_4 \text{ fault} \\ \frac{1}{T\sqrt{3}} \left| \int_0^{T/2} \frac{(T_e - T_F) k_m \sin(\omega_e t + \theta_{ej})}{\sum_{i \in S_N} k_m^2 \sin^2(\omega_e t + \theta_{ei})} dt \right|, & S_2 \text{ or } S_3 \text{ fault} \end{cases} \\ &\quad \{j \in S_F\} \end{aligned} \tag{45}$$

with

$$\begin{aligned} x &= \omega_e t \\ T &= 2\pi/\omega_e \end{aligned} \tag{46}$$

TABLE II
MAIN PARAMETERS OF THE SIX-PHASE FTPMSM

Parameters [Unit]	Value
DC bus link voltage [V]	42
Rated power [W]	25
Rated speed [rpm]	1200
Load torque [N·m]	0.2
Phase resistance [Ω]	0.76
Phase inductance [mH]	5.6

then

$$\begin{aligned} I_{\mathrm{mod1}} &= I_{\mathrm{mod2}} \\ &= \begin{cases} \frac{1}{T\sqrt{3}} \cdot \frac{T}{2\pi} \left| \int_{\pi}^{2\pi} \frac{(T_e - T_F) k_m \sin(x + \theta_{ej})}{\sum_{i \in S_N} k_m^2 \sin^2(x + \theta_{ei})} dx \right| \\ \frac{1}{T\sqrt{3}} \cdot \frac{T}{2\pi} \left| \int_{0}^{\pi} \frac{(T_e - T_F) k_m \sin(x + \theta_{ej})}{\sum_{i \in S_N} k_m^2 \sin^2(x + \theta_{ei})} dx \right| \end{cases} \\ &= \begin{cases} \frac{1}{2\sqrt{3}\pi} \left| \int_{\pi}^{2\pi} \frac{(T_e - T_F) k_m \sin(x + \theta_{ej})}{\sum_{i \in S_N} k_m^2 \sin^2(x + \theta_{ei})} dx \right|, & S_1 \text{ or } S_4 \text{ fault} \\ \frac{1}{2\sqrt{3}\pi} \left| \int_{0}^{\pi} \frac{(T_e - T_F) k_m \sin(x + \theta_{ej})}{\sum_{i \in S_N} k_m^2 \sin^2(x + \theta_{ei})} dx \right|, & S_2 \text{ or } S_3 \text{ fault} \end{cases} \\ &\quad \{j \in S_F\}. \end{aligned} \tag{47}$$

Therefore, after the single power switch open-circuit fault occurrence, the moduli of ACPV are load-dependent values and they have no relevance to the current period T, which means they are independent of the motor speed.

Then, the threshold value can be given as

$$I_{\mathrm{thres}} = k_t \ \frac{1}{2\sqrt{3}\pi} \left| \int_{\pi}^{2\pi} \frac{(T_e - T_F) k_m \sin(x + \theta_{ej})}{\sum_{i \in S_N} k_m^2 \sin^2(x + \theta_{ei})} dx \right| \quad \{j \in S_F;\ k_t \in (0, 1)\} \tag{48}$$

where k_t is the ratio between the threshold value I_{thres} I_{thres} and the module of ACPV within the range of (0,1). The ration needs to be determined based on the compromise between the rapidity and sensitivity of the diagnostic method. Low threshold value is advantageous to fast and sensitive diagnosis. However, if the threshold is too low, the probability of the misdiagnosis will increase. If the threshold value is too large, though the misdiagnosis can be avoided, the diagnostic rapidity will be affected. In this article, the value k_t is chosen to be equal to 0.9.

The k_t is determined based on the experimental tests and the practical engineering experience in order to accommodate the high transients and perform the diagnosis in a wide range of operating conditions. The flowchart of the proposed fault diagnostic approach is shown in Fig. 4, which shows the procedure of single power switch open-circuit fault detection and localization in the six-phase FTPMSM system.

IV. SIMULATION RESULTS

To verify the effectiveness of the proposed fault diagnostic approach, the simulation platform of the six-phase FTPMSM system is built, in which the main system parameters are shown

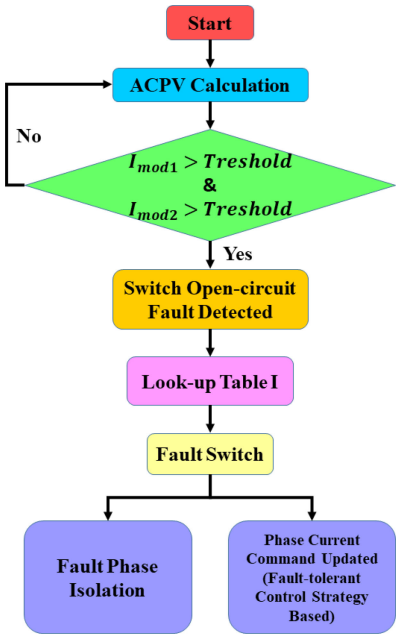

Fig. 4. Flowchart of the proposed diagnostic approach.

in Table II. The power switch open-circuit fault is simulated by sending a zero drive pulse to a designated power switch.

A. Diagnostic Results for Steady-State Working Conditions

1) Single Power Switch Open-Circuit Fault Under Normal Operation Condition: The results shown in this section are for five steady-state conditions with different speed reference and load torque. The fault power switch is taken as the MOSFET S1 of the phase-A only for demonstration purpose.

Simulation results of the fault diagnosis process of single switch open-circuit fault with rated speed reference of 1200 rpm and rated load torque of 0.2 N·m are shown in Fig. 5. As shown in Fig. 5(a), the power switch open-circuit fault occurs at $t_{\rm OC} = 200$ ms, and the torque ripple increases significantly due to the absence of fault-tolerant control algorithm. Fig. 5(b) shows the waveforms of the FTPMSM phase currents. Note that before the optimal torque control to take effect, the healthy phase current waveforms are all sinusoidal. The positive half cycle current of the fault phase-A will drop to zero after the power switch S1 open-circuit fault occurs. The waveforms of the ACPV variables $I_{\alpha 1_{\rm av}}$, $I_{\beta 1_{\rm av}}$, $I_{\rm mod1}$, $I_{\alpha 2_{\rm av}}$, $I_{\beta 2_{\rm av}}$, and $I_{\rm mod2}$ are shown in Fig. 5(c). Note that the moduli of the ACPV start increasing from nearly zero after the OC fault occurs. When the moduli of the ACPV exceed the predefined threshold, the faulty switch is then located based on the values of the ACPV and four fault-location flags are generated as shown in Fig. 5(d). Note that it takes about one fundamental current period to identify the faulty switch. Furthermore, the torque ripple can be eliminated after the fault-tolerant control strategy takes effect at $t_{\rm FT}$.

Fig. 6 show the simulation results of the fault diagnosis process of single switch open-circuit fault under the speed reference of 800 rpm and load torque of 0.2 N·m. As shown in Fig. 6(a),

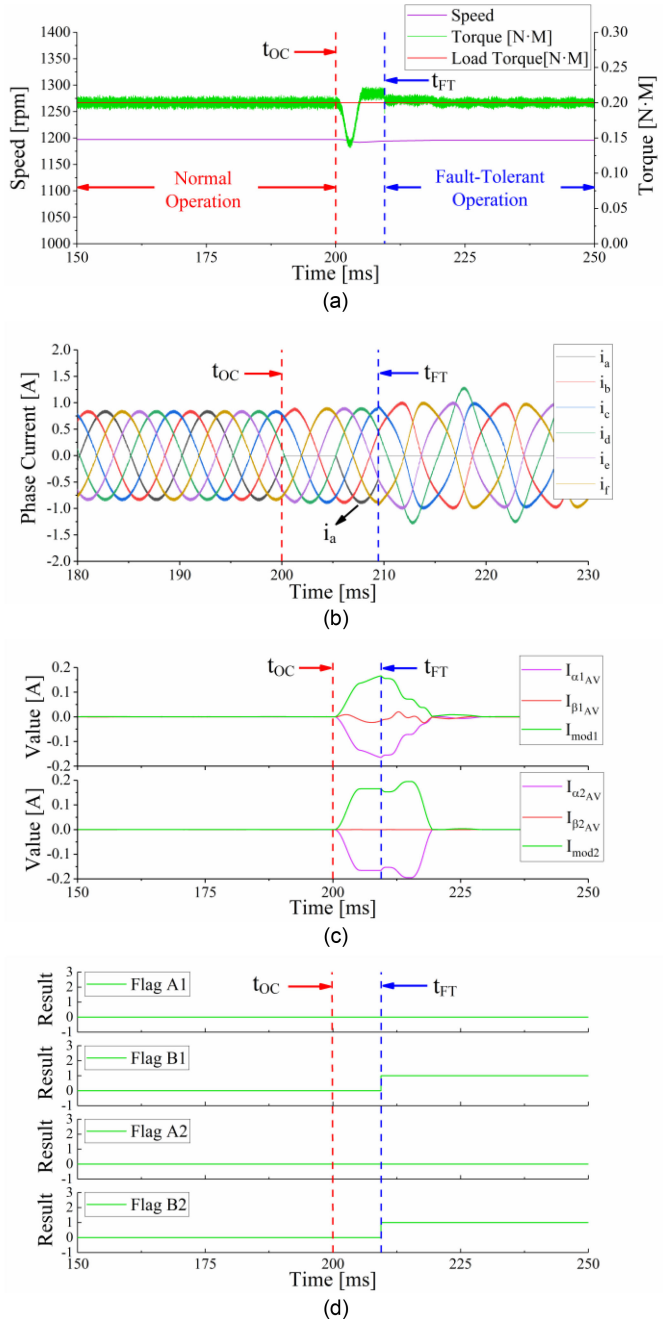

Fig. 5. Simulation results of fault diagnosis process of single switch open-circuit fault in S1 of phase-A with 1200 rpm and 0.2 N·m. (a) Speed and torque. (b) Phase currents. (c) ACPV values of $I_{\alpha 1_{\rm av}}$, $I_{\beta 1_{\rm av}}$, $I_{\rm mod1}$, $I_{\alpha 2_{\rm av}}$, $I_{\beta 2_{\rm av}}$, and $I_{\rm mod2}$. (d) Fault-location flags.

the power switch open-circuit fault occurs at $t_{\rm OC} = 200$ ms. Fig. 6(b) shows the waveforms of the FTPMSM phase currents. The waveforms of the ACPV variables $I_{\alpha 1_{\rm av}}$, $I_{\beta 1_{\rm av}}$, $I_{\rm mod1}$, $I_{\alpha 2_{\rm av}}$, $I_{\beta 2_{\rm av}}$, and $I_{\rm mod2}$ are shown in Fig. 6(c). When the moduli of the ACPV exceed the predefined threshold, the fault location flags change to "0101" from "0000", as shown in Fig. 6(d). Note that it takes about one fundamental current period of 14.5 ms to identify the faulty switch.

Similar diagnostic results can be obtained for high-speed operation with 1500 rpm and 0. 2 N·m, as shown in Fig. 7.

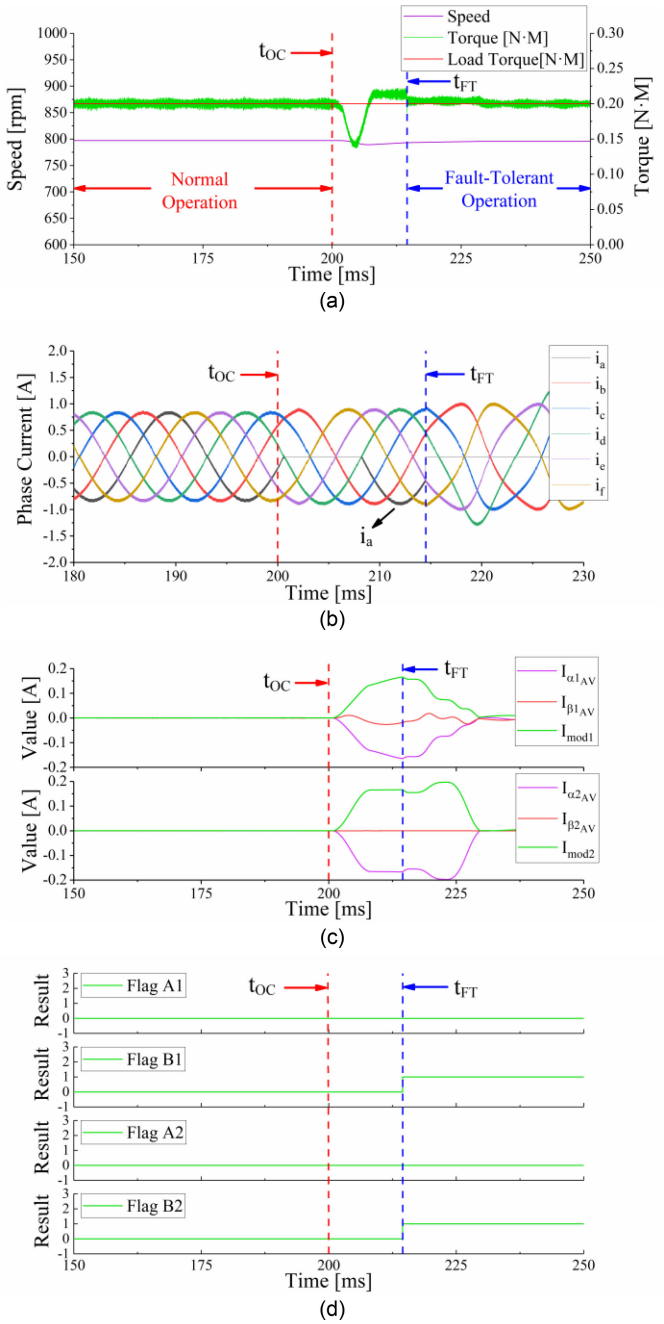

Fig. 6. Simulation results of fault diagnosis process of single switch open-circuit fault in S1 of phase-A with 800 rpm and 0.2 N·m. (a) Speed and torque. (b) Phase currents. (c) ACPV values of $I_{\alpha 1_{\mathrm{av}}}$, $I_{\beta 1_{\mathrm{av}}}$, I_{mod1}, $I_{\alpha 2_{\mathrm{av}}}$, $I_{\beta 2_{\mathrm{av}}}$, and I_{mod2}. (d) Fault-location flags.

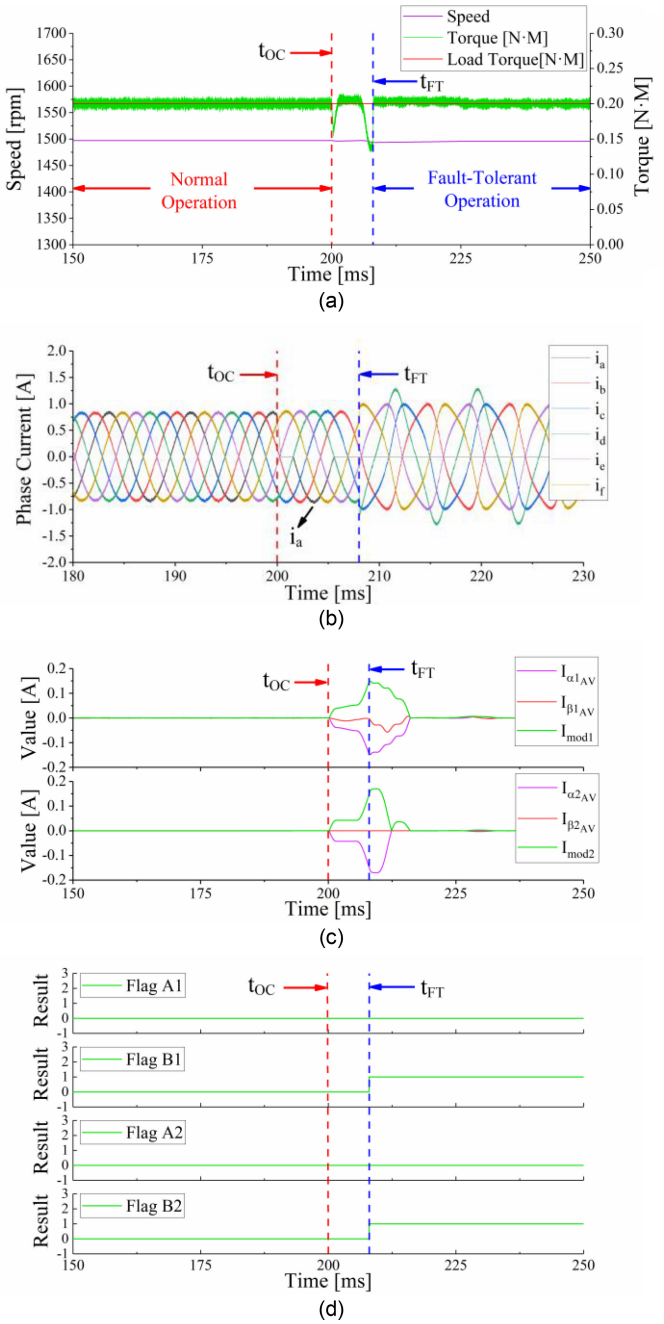

Fig. 7. Simulation results of the fault diagnosis process of single switch open-circuit fault in S1 of phase-A with 1500 rpm and 0.2 N·m. (a) Speed and torque. (b) Phase currents. (c) ACPV values of $I_{\alpha 1_{\mathrm{av}}}$, $I_{\beta 1_{\mathrm{av}}}$, I_{mod1}, $I_{\alpha 2_{\mathrm{av}}}$, $I_{\beta 2_{\mathrm{av}}}$, and I_{mod2}. (d) Fault-location flags.

For this operation point, the fundamental current period is about 8 ms, as shown in Fig. 9, respectively. As shown in Figs. 8(a) and 9(a), the power switch open-circuit fault occurs at $t_{\mathrm{OC}} = 200$ ms. The predefined threshold under high-load torque condition is three times of the low load torque condition. The fault-location flags in Figs. 8(d) and 9(d) show that they both take about one fundamental current period to identify the faulty switch.

2) Single Power Switch Open-Circuit Fault Under Single Phase Open-Circuit Fault-Tolerant Operation Condition: For the single power switch open-circuit fault simulation under one-phase open-circuit fault-tolerant operation condition, the fault power switch is taken as the MOSFET S1 of the phase-E for the six-phase FTPMSM system under phase-B open-circuit fault-tolerant operation condition. As shown in Fig. 10(a), the torque and the speed of the FTPMSM are both stable under the open-circuit fault-tolerant operation condition due to the optimal torque control. Nevertheless, the torque and the speed drop immediately after the secondary open-circuit fault occurs

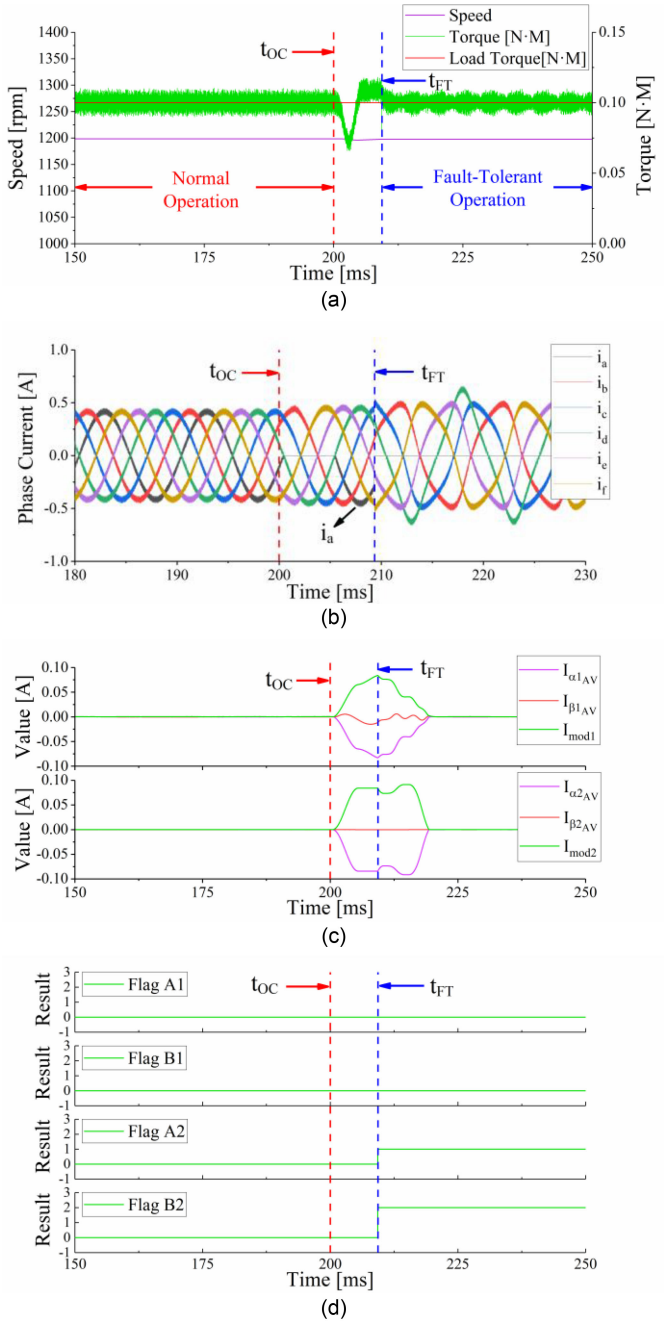

Fig. 8. Simulation results of the fault diagnosis process of single switch open-circuit fault in S1 of phase-A with 1200 rpm and 0.1 N·m. (a) Speed and torque. (b) Phase currents. (c) ACPV values of $I_{\alpha 1_{\mathrm{av}}}$, $I_{\beta 1_{\mathrm{av}}}$, I_{mod1}, $I_{\alpha 2_{\mathrm{av}}}$, $I_{\beta 2_{\mathrm{av}}}$, and I_{mod2}. (d) Fault-location flags.

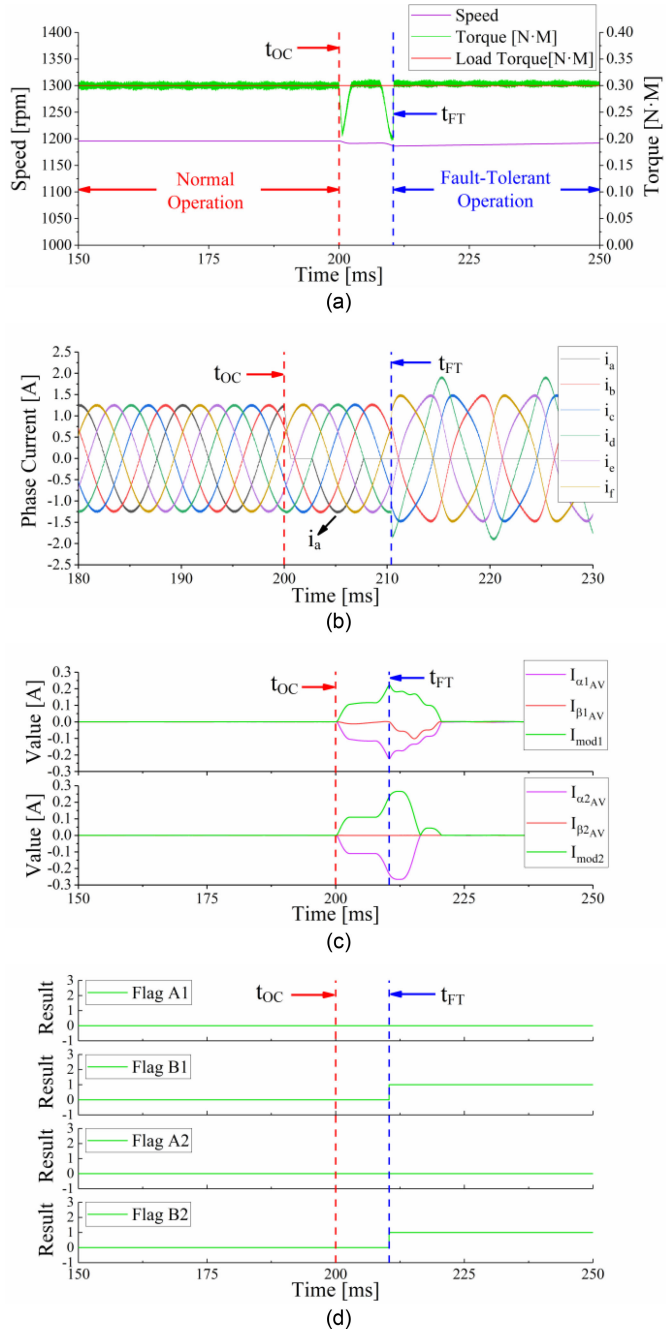

Fig. 9. Simulation results of the fault diagnosis process of single switch open-circuit fault in S1 of phase-A with 1200 rpm and 0.3 N·m. (a) Speed and torque. (b) Phase currents. (c) ACPV values of $I_{\alpha 1_{\mathrm{av}}}$, $I_{\beta 1_{\mathrm{av}}}$, I_{mod1}, $I_{\alpha 2_{\mathrm{av}}}$, $I_{\beta 2_{\mathrm{av}}}$, and I_{mod2}. (d) Fault-location flags.

at $t_{\mathrm{OC}} = 300$ ms. Fig. 10(b) shows the corresponding phase current waveforms. It can be noted that the currents in the remaining healthy phases are asymmetric and nonsinusoidal under the fault-tolerant control operation. Fig. 10(c) shows the values of the ACPV moduli under open-circuit fault-tolerant control operation, which remain at zero before the secondary fault occurs. Fig. 10(d) shows the fault-location flags. Note that when the power switch open-circuit fault occurs under one phase open-circuit fault-tolerant operation condition, the fault-location flags change from "0000" to "2220," which in turns means that the fault power switch is MOSFET S1 or S4 of phase-E from Table I.

3) Single Power Switch Open-Circuit Fault Under Single Phase Short-Circuit Fault-Tolerant Operation Condition: For the single power switch, open-circuit fault simulation under one-phase short-circuit fault-tolerant operation condition, the fault power switch is taken as the MOSFET S1 of the phase-E for the six-phase FTPMSM system under phase-B short-circuit

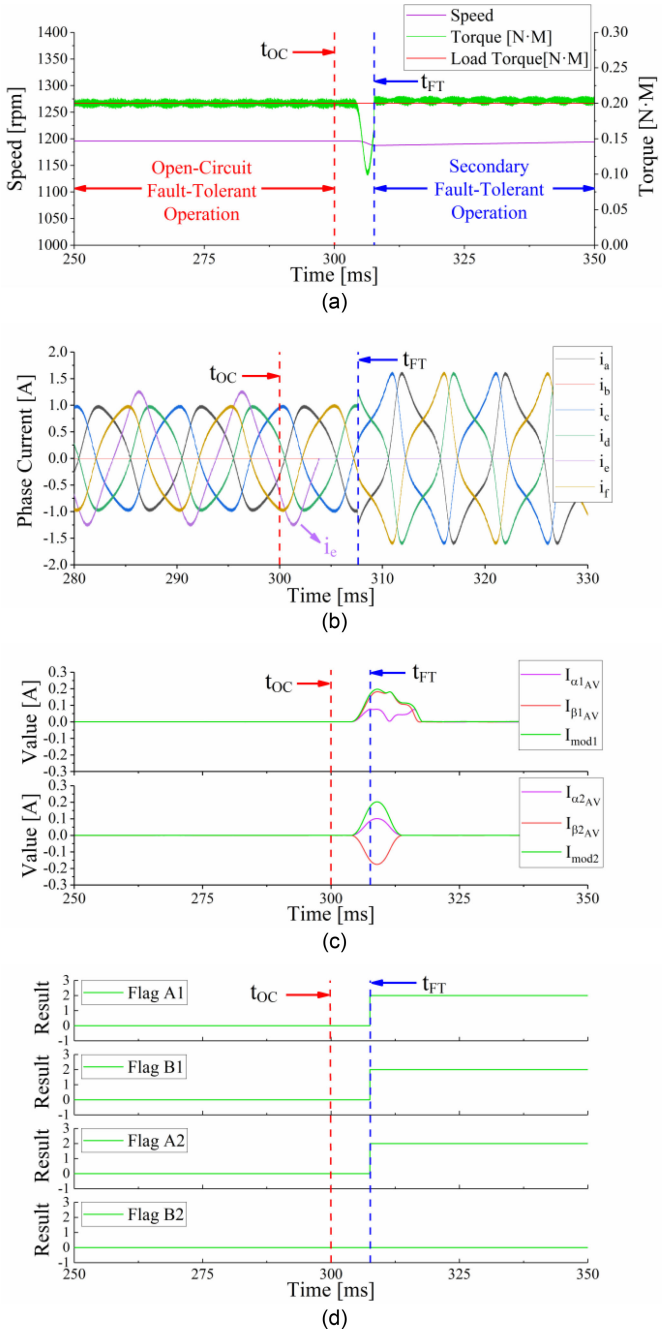

Fig. 10. Simulation results of the fault diagnosis process of secondary single switch open-circuit fault in S1 of phase-E under phase-B open-circuit fault-tolerant operation condition with 1200 rpm and 0.2 N·m. (a) Speed and torque. (b) Phase currents. (c) ACPV values of $I_{\alpha 1_{\rm av}}$, $I_{\beta 1_{\rm av}}$, $I_{\rm mod1}$, $I_{\alpha 2_{\rm av}}$, $I_{\beta 2_{\rm av}}$, and $I_{\rm mod2}$. (e) Fault-location flags.

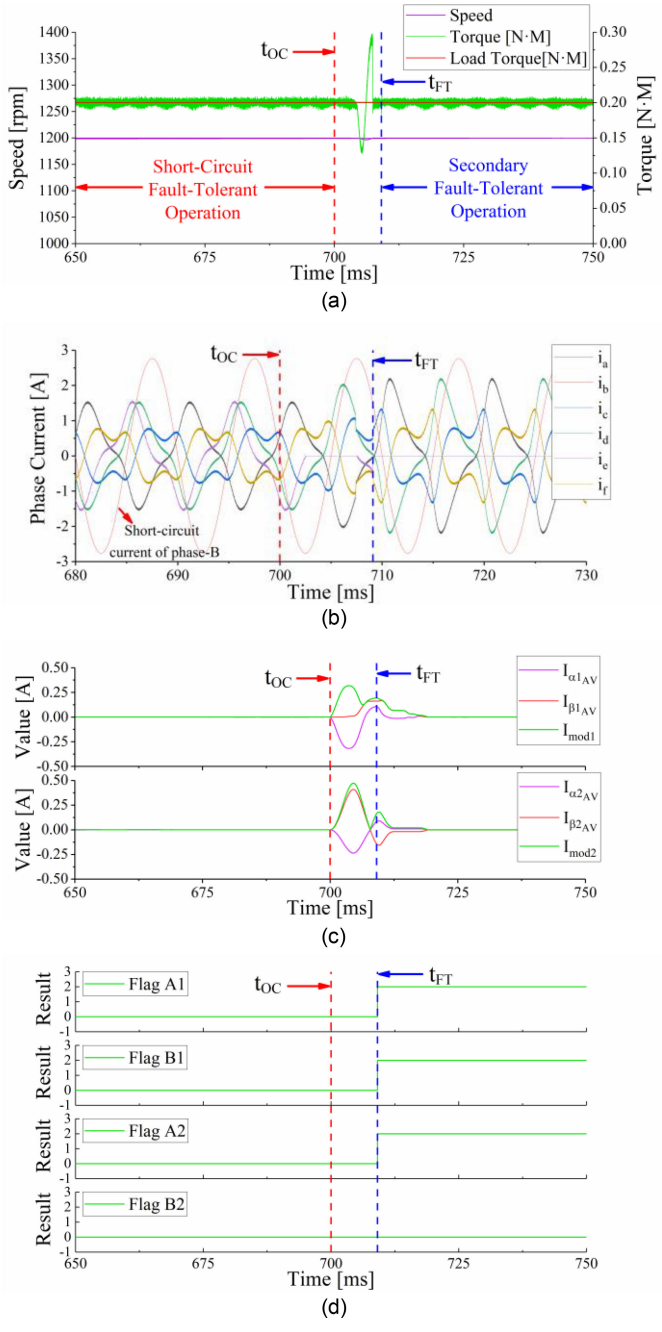

Fig. 11. Simulation results of the fault diagnosis process of secondary single switch open-circuit fault in S1 of phase-E under phase-B short-circuit fault-tolerant operation condition with 1200 rpm and 0.2 N·m. (a) Speed and torque. (b) Phase currents. (c) ACPV values of $I_{\alpha 1_{\rm av}}$, $I_{\beta 1_{\rm av}}$, $I_{\rm mod1}$, $I_{\alpha 2_{\rm av}}$, $I_{\beta 2_{\rm av}}$, and $I_{\rm mod2}$. (e) Fault-location flags.

fault-tolerant operation condition. Fig. 11(a) shows the torque and speed trajectories of the six-phase FTPMSM system. The FTPMSM system can operate steadily under one-phase short-circuit condition, while the optimal torque control is used to eliminate the torque ripple caused by the phase short-circuit fault. After the power switch open-circuit fault occurs in MOSFET S1 of phase-E at $t_{\rm OC} = 700$ ms, there will generate a large torque ripple in the fault transient process. Fig. 11(b) shows the corresponding phase current waveforms. Note that the amplitude of the short-circuit current in phase-B is 2.8 A. In addition, under the short-circuit fault-tolerant control operation, the currents in healthy phases are both nonsinusoidal. Fig. 11(c) shows the values of the ACPV under short-circuit fault-tolerant control operation, which will deviate from the zero as the fault occurs. Fig. 11(d) shows the corresponding fault location flags. Note that after about one fundamental current period, the fault location

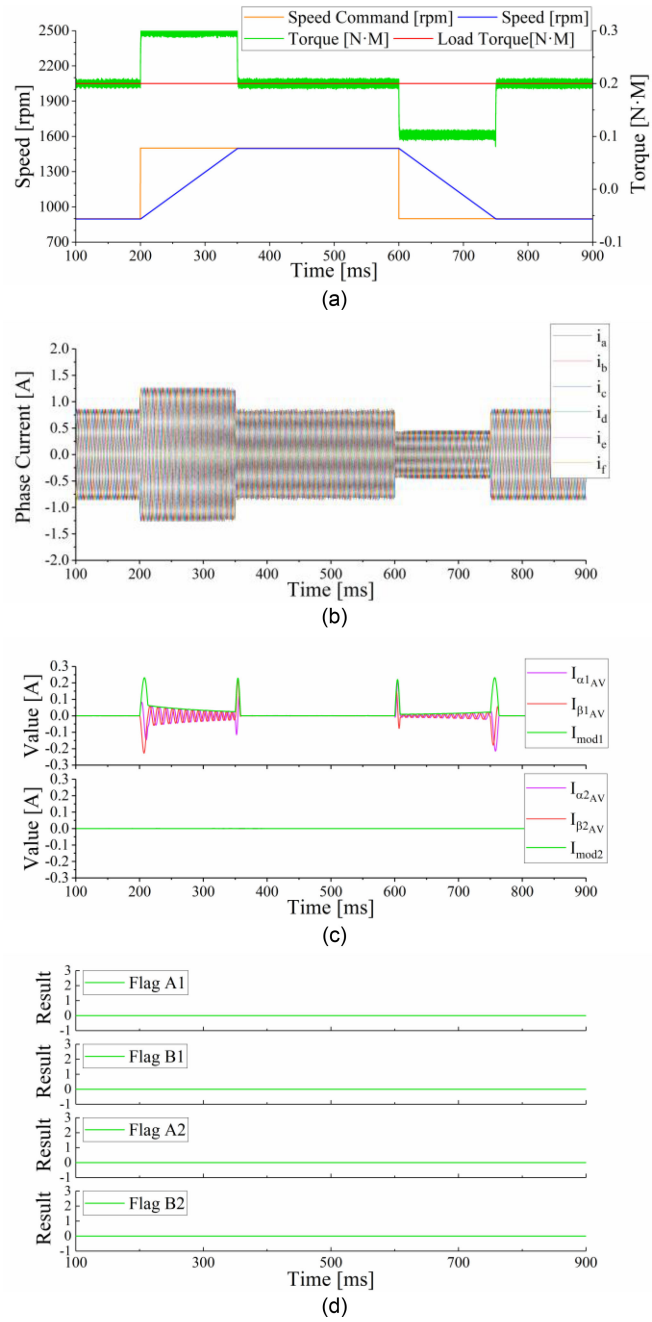

Fig. 12. Simulation results of robustness of the proposed approach under speed variations. (a) Speed and torque. (b) Phase currents. (c) ACPV values of $I_{\alpha 1_{\mathrm{av}}}$, $I_{\beta 1_{\mathrm{av}}}$, I_{mod1}, $I_{\alpha 2_{\mathrm{av}}}$, $I_{\beta 2_{\mathrm{av}}}$, and I_{mod2}. (d) Fault-location flags.

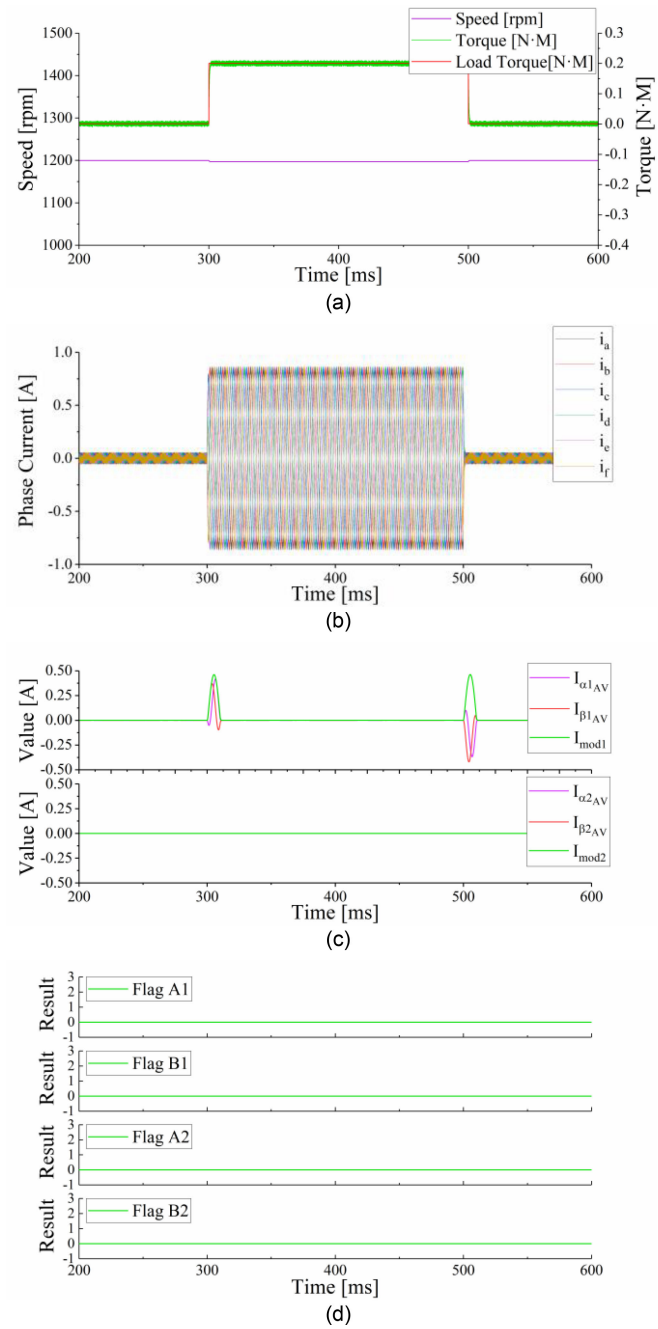

Fig. 13. Simulation results of robustness of the proposed approach under load torque variations. (a) Speed and torque. (b) Phase currents. (c) ACPV values of $I_{\alpha 1_{\mathrm{av}}}$, $I_{\beta 1_{\mathrm{av}}}$, I_{mod1}, $I_{\alpha 2_{\mathrm{av}}}$, $I_{\beta 2_{\mathrm{av}}}$, and I_{mod2}. (d) Fault-location flags.

flags are changed to "2220." Therefore, the fault power switch is located as MOSFET S1 or S4 of phase-E from Table I.

B. Performance Evaluation Under Transient Working Conditions

To accomplish the evaluation of the proposed diagnostic method under transient conditions, load and speed variations are tested. The simulation is addressed in Figs. 12 and 13 to verify the robustness of the proposed diagnostic method.

1) Diagnostic Performance Under Speed Variations: In Fig. 12, a constant rated load torque is imposed and two instantaneous speed changes are introduced. At $t = 200$ ms, a speed step from 900 to 1500 rpm is imposed. The second speed step from 1500 to 900 rpm is imposed at $t = 600$ ms. Fig. 12(a) shows the behavior of the motor. As it can be seen in Fig. 12(b), the phase currents increase significantly during the acceleration process. Meanwhile, there is a large decrease in the phase currents during the deceleration process. Note that the ACPV value of I_{mod1} in Fig. 12(c) exceeds the threshold value during the transients.

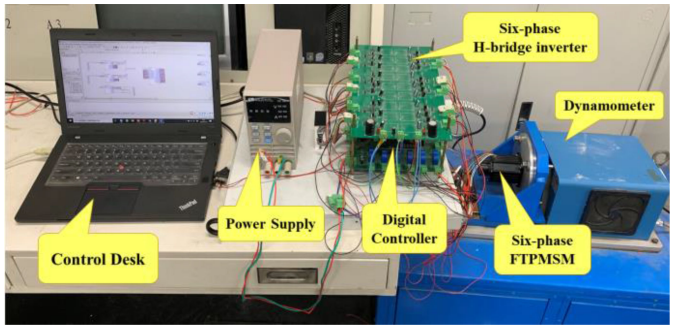

Fig. 14. General view of the experimental platform.

However, the value of I_{mod2} remains at almost zero, preventing the generation of any false fault detection. As can be confirmed by the location flags shown in Fig. 12(d), where their values are always "0000."

2) Diagnostic Performance Under Load Torque Variations: The rated reference speed of 1200 rpm is imposed for the results shown in Fig. 13, and two load steps are introduced. At $t =$ 300 ms the load torque increases from no-load condition to rated load torque, which results in an evident increase of the motor phase currents, as shown in Fig. 13(b). The reverse load step, from rated load torque to no-load condition, is forced at $t = 500$ ms. Consequently, the phase currents turn into almost null in a short period of time, imposing a great challenge to the robustness of the diagnostic method. Note that the ACPV value of I_{mod1} exceed the threshold value during transients. Nevertheless, the ACPV value of I_{mod2} remains at almost zero, which prevents a misinterpretation of the load torque variation. Therefore, as shown in Fig. 13(d), all the location flags remain zero during the whole process.

V. Experimental Results

To verify the effectiveness of the proposed fault diagnostic method, the experimental platform of the six-phase FTPMSM system is established, as shown in Fig. 14, which consists of the six-phase FTPMSM, digital controller, H-bridge based fault-tolerant driver, power supply, dynamometer, and host computer. The main system parameters are shown in Table II.

The sample rates of the current loop and the speed loop are 25 and 100 us, respectively. The switching frequency of the system is 40 kHz. The power switch open-circuit fault emulation is conducted by setting its drive pulse as zero. The one phase open-circuit fault emulation is performed by turning OFF all the four MOSFET power switches of the H-bridge inverter. The one phase short-circuit fault emulation is performed by turning OFF the two high-side MOSFET power switches of the H-bridge inverter and turning on the two low-side MOSFET power switches.

A. Diagnostic Results for Steady-State Working Conditions

1) Single Power Switch Open-Circuit Fault Under Normal Operation Condition: Corresponding to the simulation results, the experimental results shown in this section are for five steady-state conditions with different speed reference and load torque as well. The fault power switch is also taken as the MOSFET S1 of the phase-A.

Fig. 15 shows the fault diagnosis process for the six-phase FTPMSM system under the normal condition with the open-circuit fault occurrence in power MOSFET S1 of phase-A with rated speed reference of 1200 rpm and rated load torque of 0.2 N·m. As shown in Fig. 15(a) and 15(b), before the power switch open-circuit fault occurs, the phase current waveforms are almost sinusoidal with a fundamental current period around 10 ms. After the open-circuit fault occurrence for the power MOSFET S1 of phase-A, the moduli of ACPV will increase rapidly as shown in Fig. 15(c) and (d). When the moduli of ACPV are higher than the threshold, the power switch open-circuit fault is confirmed. Then by the fault location flags, the fault power switch can be located. As shown in Fig. 15(e) and (f), after the fault occurrence, the fault location flags change to "0101" from "0000," which means that the fault power switch is MOSFET S1 or S4 of phase-A from Table I. It can be seen that it takes about one fundamental current period of 10 ms to identify the specific fault.

Fig. 16 shows the fault diagnosis process of a single power switch open-circuit fault under the speed reference of 800 rpm and load torque of 0.2 N·m. Fig. 16(a) and (b) show that the fundamental current period is around 15 ms. As shown in Fig. 16(c) and (d), the trends of the ACPV variables $I_{\alpha 1_{\mathrm{av}}}$, $I_{\beta 1_{\mathrm{av}}}$, I_{mod1}, $I_{\alpha 2_{\mathrm{av}}}$, $I_{\beta 2_{\mathrm{av}}}$, and I_{mod2} are same as the condition in Fig. 15. Meanwhile, with the same predefined threshold, the fault location flags change to "0101" from "0000" when the fault power switch is located. Note that it takes about 15.4 ms to locate the faulty switch.

The diagnostic results of single power switch open-circuit fault under high-speed operation with 1500 rpm and 0. 2 N·m is shown in Fig. 17. The waveforms of the phase currents in Fig. 17(a) and (b) show that the fundamental current period is about 8 ms. It can be noted that the values of the ACPV variables $I_{\alpha 1_{\mathrm{av}}}$, $I_{\beta 1_{\mathrm{av}}}$, I_{mod1}, $I_{\alpha 2_{\mathrm{av}}}$, $I_{\beta 2_{\mathrm{av}}}$, and I_{mod2} in Fig. 17(c) and (d) are similar to the previous two operation conditions, which indicates that the values of the ACPV variables are load dependent and they have no relevance to the motor speed. As shown in Fig. 17(e) and (f), the open-circuit fault occurs when the fault flag change from "0" to "1." When the faulty switch is located, the fault location flags change to "0101" from "0000," which takes approximately 7.5 ms.

Figs. 18 and 19 show the experimental results regarding the single switch open-circuit fault under low load torque of 0.1 N·m and high load torque of 0.3 N·m, respectively, both with rated speed reference of 1200 rpm. The waveforms of the phase currents in Figs. 18(a), (b) and 19(a), (b) show that the currents have different amplitudes but the same periods under different load torques. Correspondingly, after the power switch open-circuit fault occurs, the values of the ACPV variables under high load torque are obviously larger than that of the low load torque condition, as shown in Figs. 18(c), (d) and 19(c), (d). The predefined threshold under high load torque condition is three times of the low load torque condition. With identical open-circuit fault power switch, the fault location flags in Figs. 18(e), (f) and 19(e), (f) show that they both change from

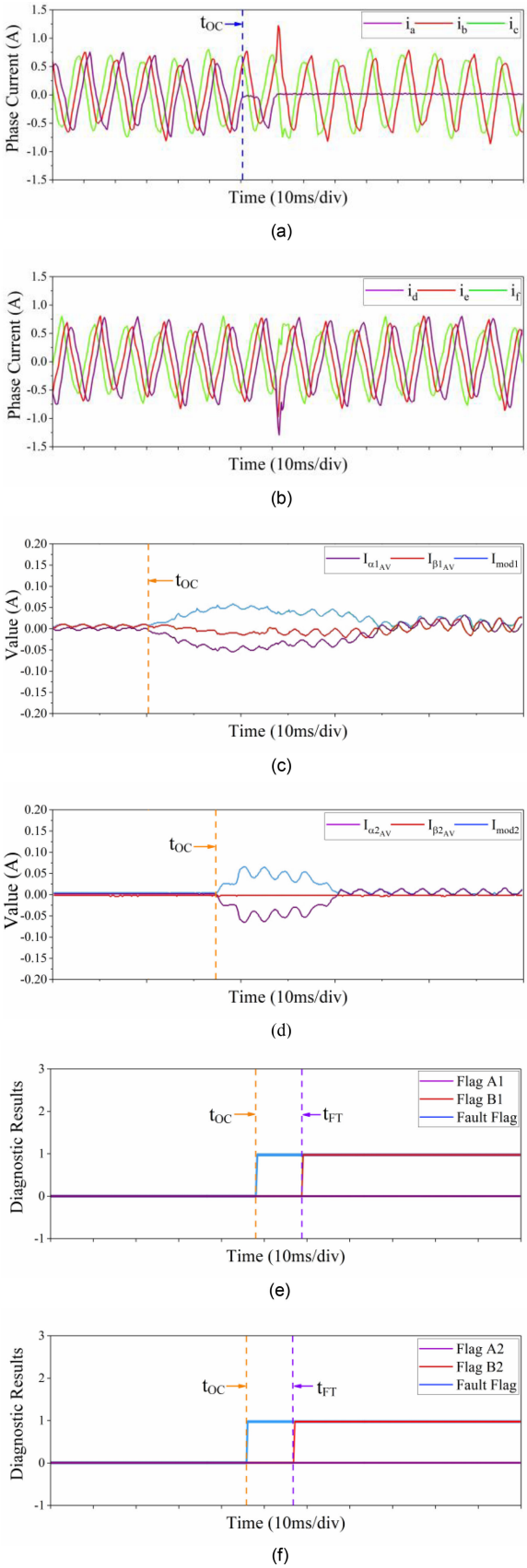

Fig. 15. Experimental results of fault diagnosis process of single switch open-circuit fault in S1 of phase-A with 1200 rpm and 0.2 N·m. (a) Phase currents of A, B, and C. (b) Phase currents of D, E, and F. (c) ACPV values of $I_{\alpha 1_{av}}$, $I_{\beta 1_{av}}$, I_{mod1}. (d) ACPV values of $I_{\alpha 2_{av}}$, $I_{\beta 2_{av}}$, I_{mod2}. (e) and (f) Open-circuit fault flag and fault location flags.

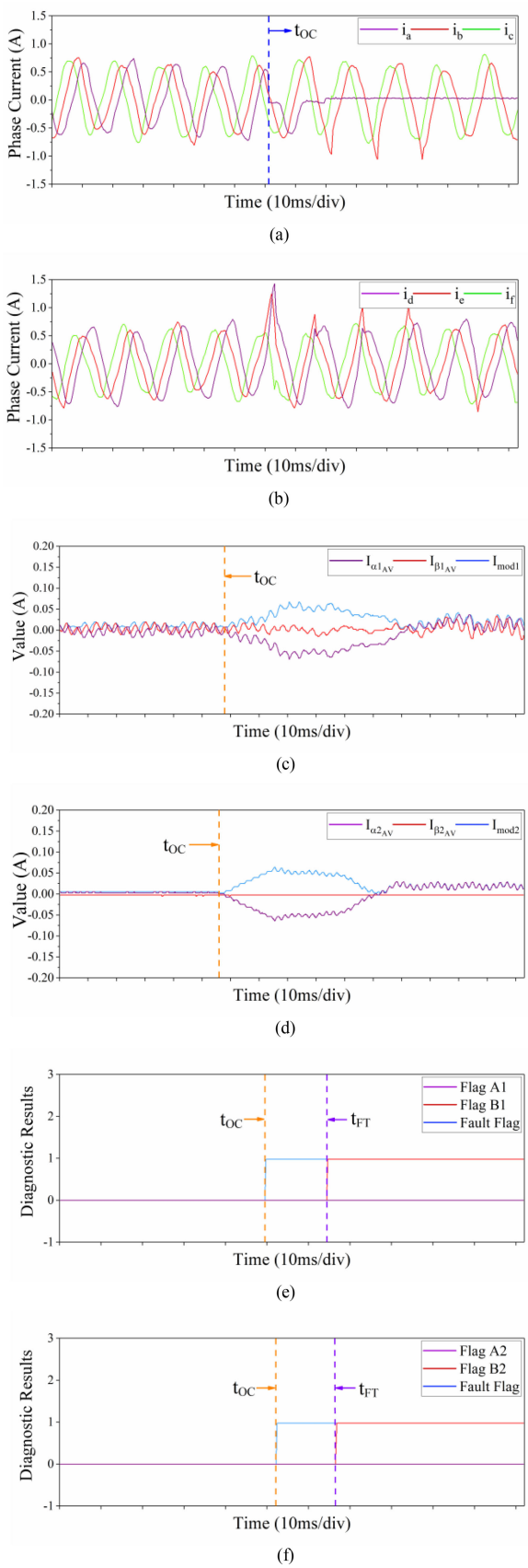

Fig. 16. Experimental results of fault diagnosis process of single switch open-circuit fault in S1 of phase-A with 800 rpm and 0.2 N·m. (a) Phase currents of A, B, C. (b) Phase currents of D, E, F. (c) ACPV values of $I_{\alpha 1_{av}}$, $I_{\beta 1_{av}}$, I_{mod1}. (d) ACPV values of $I_{\alpha 2_{av}}$, $I_{\beta 2_{av}}$, I_{mod2}. (e) and (f) Open-circuit fault flag and fault location flags.

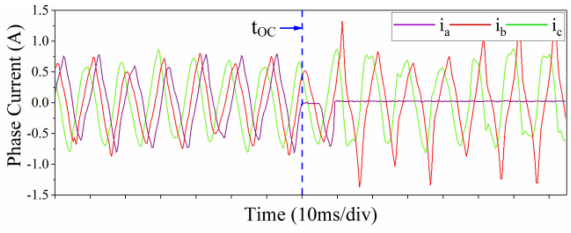

(a)

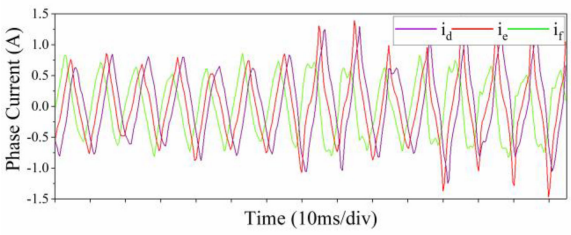

(b)

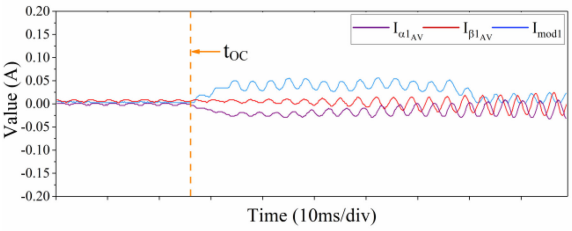

(c)

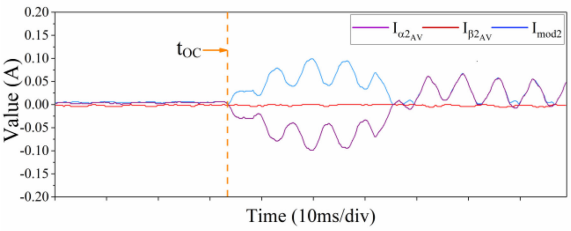

(d)

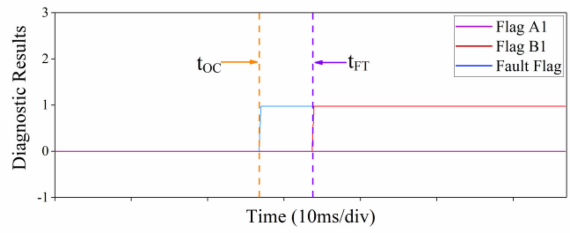

(e)

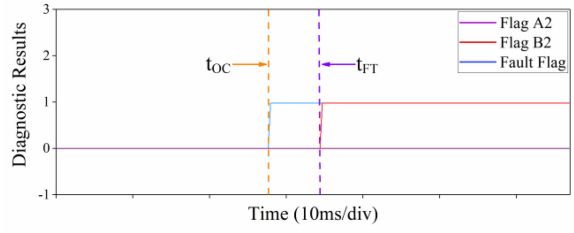

(f)

Fig. 17. Experimental results of the fault diagnosis process of single switch open-circuit fault in S1 of phase-A with 1500 rpm and 0.2 N·m. (a) Phase currents of A, B, and C. (b) Phase currents of D, E, and F. (c) ACPV values of $I_{\alpha 1_{av}}$, $I_{\beta 1_{av}}$, and I_{mod1}. (d) ACPV values of $I_{\alpha 2_{av}}$, $I_{\beta 2_{av}}$, and I_{mod2}. (e) and (f) Open-circuit fault flag and fault location flags.

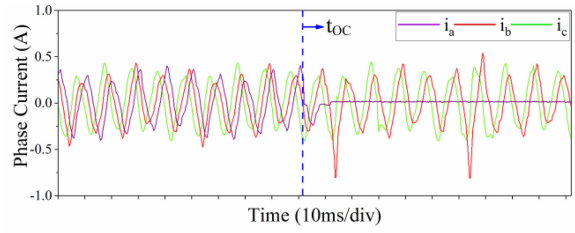

(a)

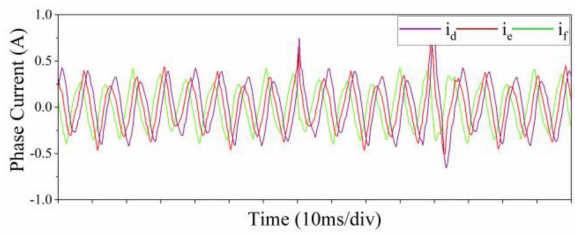

(b)

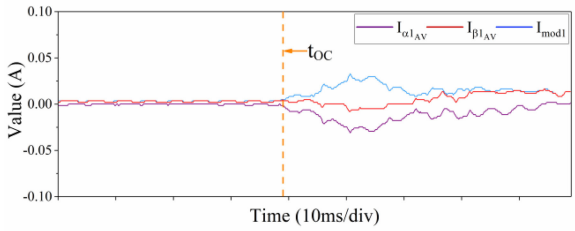

(c)

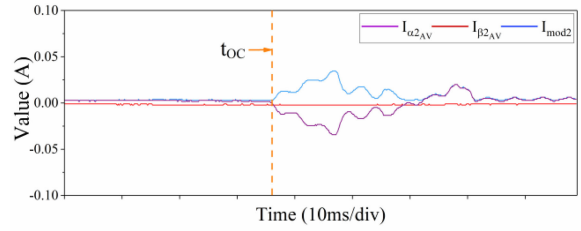

(d)

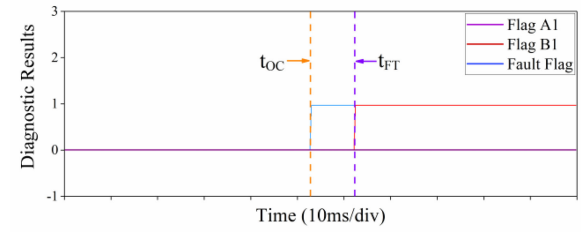

(e)

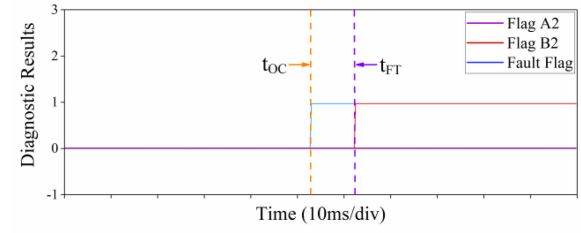

(f)

Fig. 18. Experimental results of the fault diagnosis process of single switch open-circuit fault in S1 of phase-A with 1200 rpm and 0.1 N·m. (a) Phase currents of A, B, and C. (b) Phase currents of D, E, and F. (c) ACPV values of $I_{\alpha 1_{av}}$, $I_{\beta 1_{av}}$, and I_{mod1}. (d) ACPV values of $I_{\alpha 2_{av}}$, $I_{\beta 2_{av}}$, and I_{mod2}. (e) and (f) Open-circuit fault flag and fault location flags.

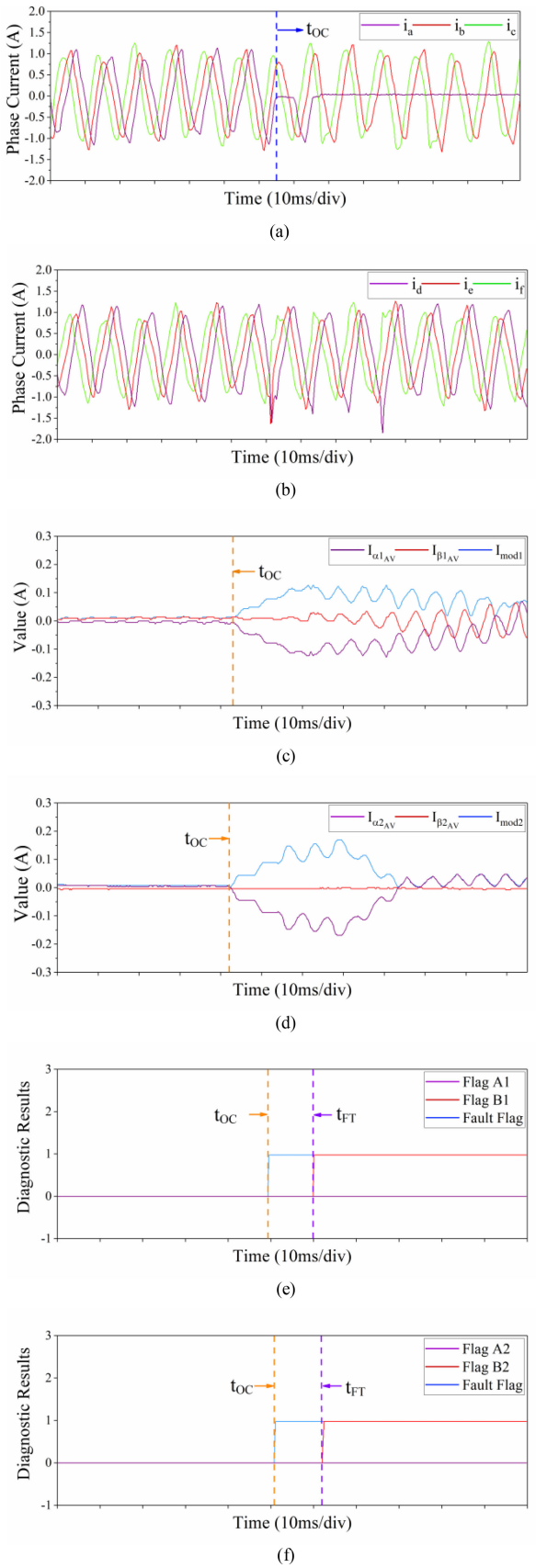

Fig. 19. Experimental results of the fault diagnosis process of single switch open-circuit fault in S1 of phase-A with 1200 rpm and 0.3 N·m. (a) Phase currents of A, B, and C. (b) Phase currents of D, E, and F. (c) ACPV values of $I_{\alpha 1_{\mathrm{av}}}$, $I_{\beta 1_{\mathrm{av}}}$, and I_{mod1}. (d) ACPV values of $I_{\alpha 2_{\mathrm{av}}}$, $I_{\beta 2_{\mathrm{av}}}$, and I_{mod2}. (e) and (f) Open-circuit fault flag and fault location flags.

"0000" to "0101" after the fault occurrence and they both take about 10 ms to identify the faulty switch.

2) Single Power Switch Open-Circuit Fault Under Single Phase Open-Circuit Fault-Tolerant Operation Condition: Fig. 20 shows the power MOSFET S1 of phase-E open-circuit fault diagnosis process for the six-phase FTPMSM system under phase-B open-circuit fault-tolerant operation condition. During one phase open-circuit fault-tolerant operation condition, the remaining healthy phase currents are nonsinusoidal, as shown in Fig. 20(a) and (b), which prevents all the existing fault diagnosis method from being directly applied. Fig. 20(c) and (d) shows the moduli of the ACPV, which remains nearly at zero during the phase open-circuit fault-tolerant operation, same as the normal operation condition. The moduli of the ACPV increases immediately after the secondary open-circuit fault occurs and it takes less than two fundamental current period to locate the faulty switch.

As shown in Fig. 20(e) and (f), the fault location flags are generated at t_{FT} basing on the values of $I_{\alpha 1_{\mathrm{av}}}$, $I_{\beta 1_{\mathrm{av}}}$, $I_{\alpha 2_{\mathrm{av}}}$, and $I_{\beta 2_{\mathrm{av}}}$, which changes to "2220" from "0000." According to Table I, the fault power MOSFET can be located as MOSFET S1 or S4 of phase-E.

3) Single Power Switch Open-Circuit Fault Under Single Phase Short-Circuit Fault-Tolerant Operation Condition: Fig. 21 shows the power MOSFET S1 of phase-E open-circuit fault diagnosis process for the six-phase FTPMSM system under phase-B short-circuit fault-tolerant operation condition. To eliminate the torque ripple in fault-tolerant operation condition, the remaining healthy phase currents are seriously distorted, as shown in Fig. 21(a) and (b), while the amplitude of the steady short-circuit current in phase-B is about 2.75 A. Fig. 21(c) and (d) shows the corresponding values of ACPV. Note that the values of ACPV modulus are near zero during the fault-tolerant operation condition. After the power switch open-circuit fault occurrence, the values of ACPV moduli increase rapidly above the fault detection threshold. Fig. 21(e) and (f) shows the corresponding fault location flags. Note that after the fault occurrence, the fault location flags changes to "2220" from "0000" in about 1.5 times of the fundamental current period. Therefore, the fault power MOSFET can be determined as MOSFET S1 or S4 of phase-E based on Table I.

B. Performance Evaluation Under Transient Working Conditions

To verify the robustness of the proposed diagnostic method under transient conditions, speed and load variations are tested. In addition, all the power switches are healthy in the tests. Since the current of each phase is symmetrical, only three phase currents are presented here for demonstration purpose.

1) Diagnostic Performance Under Speed Variations: The experimental results of the diagnostic performance under speed variations are illustrated in Fig. 22. A constant load torque of 0.2 N·m is imposed during the whole process. As can be seen in Fig. 22(a), the speed command steps from 800 to 1500 rpm first. The second speed command step from 1500 to 800 rpm is introduced when the motor's actual speed reaches 1500 rpm. Fig. 22(b) shows that not only the period of the phase current

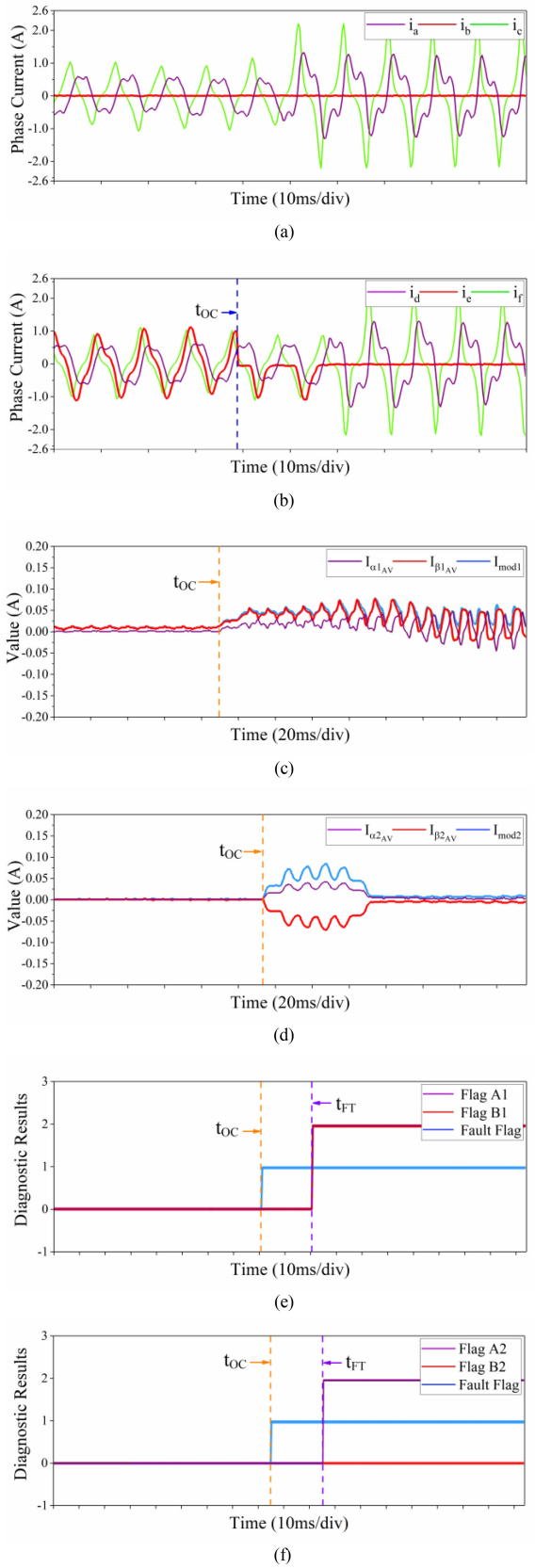

Fig. 20. Experimental results of the fault diagnosis process of secondary single power switch open-circuit fault in S1 of phase-E under phase-B open-circuit fault-tolerant operation condition with 1200 rpm and 0.2 N·m. (a) Phase currents of A, B, and C. (b) Phase currents of D, E, and F. (c) ACPV values of $I_{\alpha 1_{\mathrm{av}}}$, $I_{\beta 1_{\mathrm{av}}}$, and I_{mod1}. (d) ACPV values of $I_{\alpha 2_{\mathrm{av}}}$, $I_{\beta 2_{\mathrm{av}}}$, and I_{mod2}. (e) and (f) Open-circuit fault flag and fault-location flags.

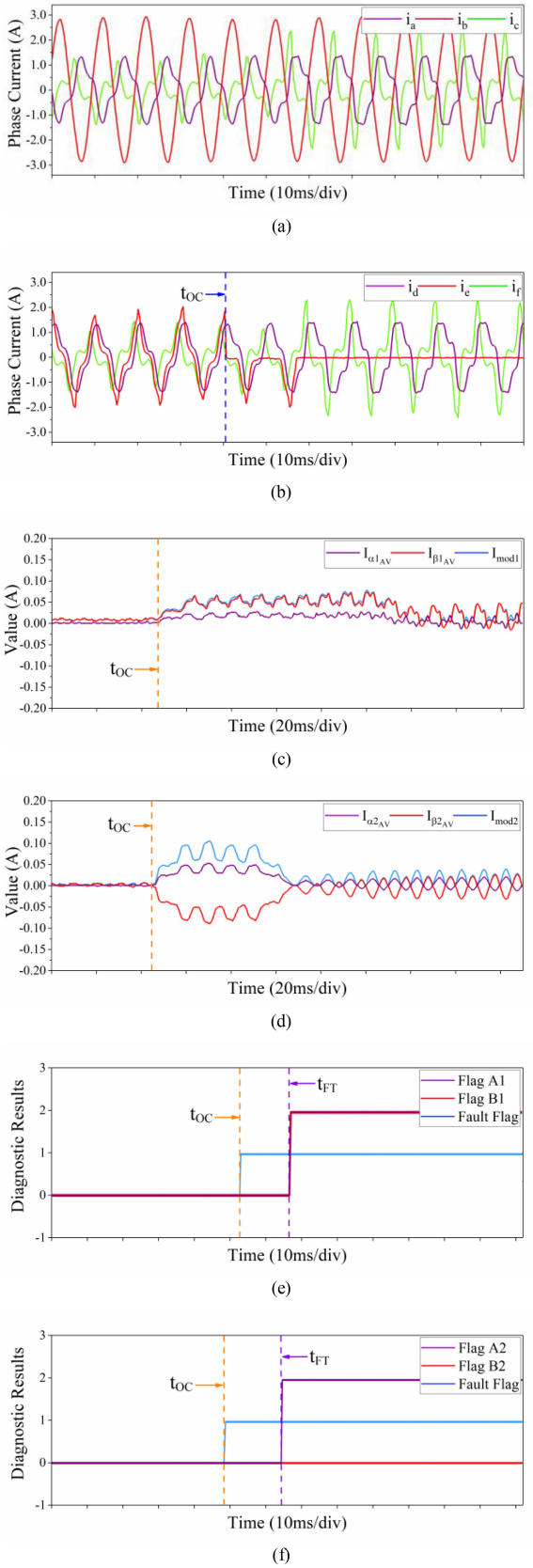

Fig. 21. Experimental results of fault diagnosis process of secondary single power switch open-circuit fault in S1 of phase-E under phase-B short-circuit fault-tolerant operation condition with 1200 rpm and 0.2 N·m. (a) Phase currents of A, B, and C. (b) Phase currents of D, E, and F. (c) ACPV values of $I_{\alpha 1_{\mathrm{av}}}$, $I_{\beta 1_{\mathrm{av}}}$, and I_{mod1}. (d) ACPV values of $I_{\alpha 2_{\mathrm{av}}}$, $I_{\beta 2_{\mathrm{av}}}$, and I_{mod2}. (e) and (f) Open-circuit fault flag and fault-location flags.

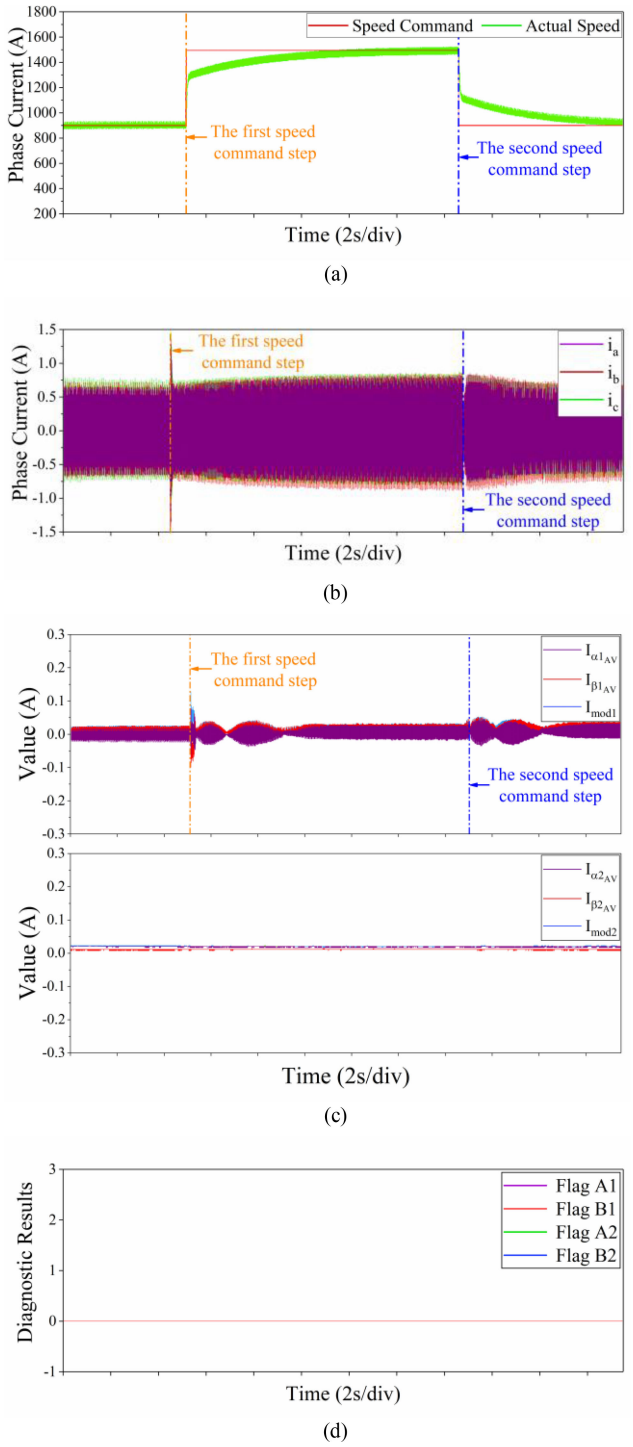

Fig. 22. Experimental results of robustness of the proposed approach under speed variations. (a) Motor speed. (b) Phase currents of A, B, and C. (c) ACPV values of $I_{\alpha 1_{\mathrm{av}}}$, $I_{\beta 1_{\mathrm{av}}}$, I_{mod1}, $I_{\alpha 2_{\mathrm{av}}}$, $I_{\beta 2_{\mathrm{av}}}$, and I_{mod2}. (d) Fault-location flags.

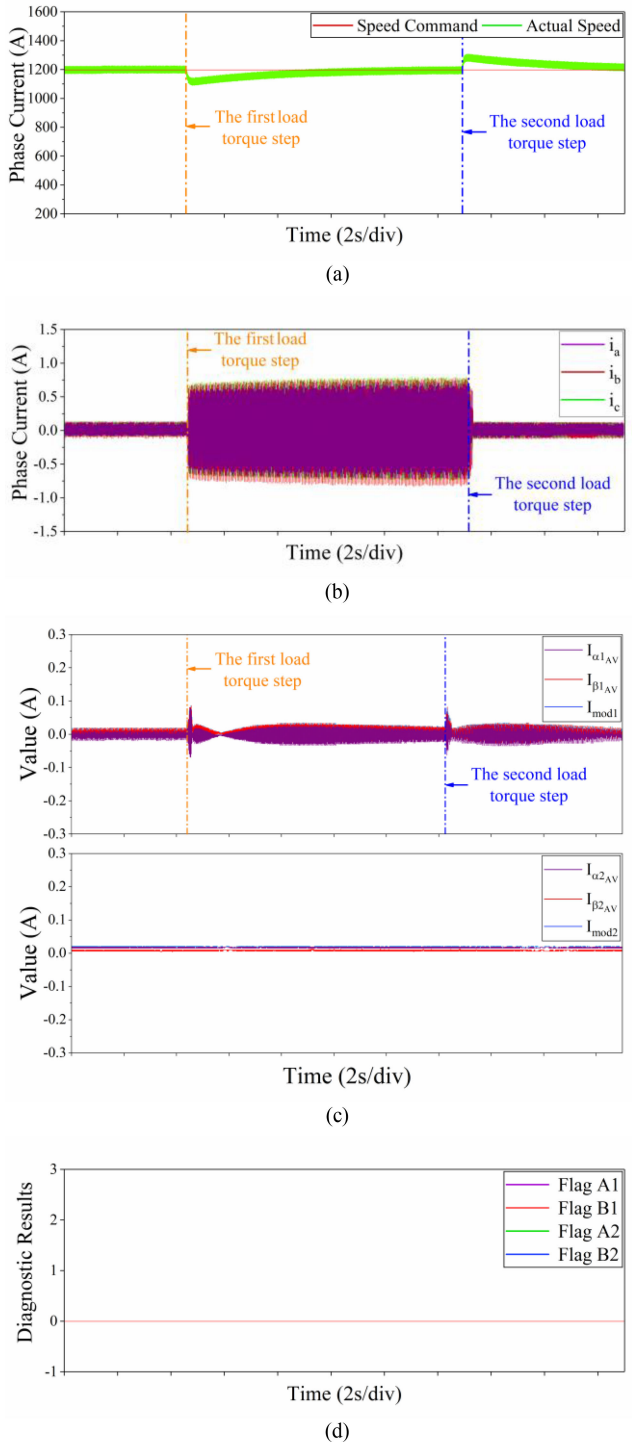

Fig. 23. Experimental results of robustness of the proposed approach under load torque variations. (a) Motor speed. (b) Phase currents of A, B, and C. (c) ACPV values of $I_{\alpha 1_{\mathrm{av}}}$, $I_{\beta 1_{\mathrm{av}}}$, I_{mod1}, $I_{\alpha 2_{\mathrm{av}}}$, $I_{\beta 2_{\mathrm{av}}}$, and I_{mod2}. (d) Fault-location flags.

changes during speed variations but also the amplitude of the current changes drastically when the speed command changes abruptly. The values of the ACPV variables $I_{\alpha 1_{\mathrm{av}}}$, $I_{\beta 1_{\mathrm{av}}}$, I_{mod1}, $I_{\alpha 2_{\mathrm{av}}}$, $I_{\beta 2_{\mathrm{av}}}$, and I_{mod2} are shown in Fig. 22(c). It can be noted that the ACPV value of $I_{\alpha 1_{\mathrm{av}}}$, $I_{\beta 1_{\mathrm{av}}}$, and I_{mod1} shows obvious fluctuation and I_{mod1} exceeds the threshold value during the transients. Nevertheless, the ACPV value of $I_{\alpha 2_{\mathrm{av}}}$, $I_{\beta 2_{\mathrm{av}}}$, and I_{mod2} remains at zero throughout the transients. Therefore, according to the condition judgment of the occurrence of the open-circuit fault, no fault detection will be generated and the four location flags in Fig. 22(d) are always "0000."

2) Diagnostic Performance Under Load Torque Variations: Fig. 23 shows the experimental results of the diagnostic performance under load torque variations. A constant speed command of 1200 rpm is imposed during the whole process and two load steps are introduced. Fig. 23(a) shows the speed of the motor when it operates at 1200 rpm with no load before the first load step. The speed is reduced about 100 rpm when the load torque changes to 0.2 N·m and it increases immediately after the load torque changes back to 0 N·m. As it can be seen in Fig. 23(b), there is a sharp increase and decrease in the phase currents under the two load torque steps, respectively. Similar to the speed variations condition, as illustrated in Fig. 23(c), the ACPV value of I_{mod1} exceeds the threshold during the transients while the ACPV value of I_{mod2} remains at almost zero, which prevents a misinterpretation of the load torque variation. It can be confirmed in Fig. 23(d) that all the location flags remain "0000" which means that no false diagnostics is emitted.

VI. Conclusion

This article proposes a new ACPV-based power switch open-circuit fault diagnosis for the six-phase FTPMSM system in normal and phase open-circuit/short-circuit fault-tolerant operation conditions, which was not available earlier. First, the fault diagnostic method is proposed to detect the power switch open-circuit fault based on the moduli of the ACPV in two orthogonal subspaces. Second, the ACPV-based fault location approach is proposed to identify the fault power switch according to the sign symbol of the ACPV. The resulting fault diagnosis approach has simple structure, low computation burden, rapid diagnosis, and no extra hardware cost, which can detect the power switch open-circuit fault online for the FTPMSM system in both normal and fault-tolerant operation conditions.

The novelty of this article is the first time to propose a new online power switch open-circuit fault diagnosis approach for the FTPMSM system in phase open-circuit and short-circuit fault-tolerant operation conditions, which lays the foundation for the continuous operation of the FTPMSM system with multiple fault condition. That is, the proposed approach can detect the second fault of the FTPMSM from the phase open-circuit/short-circuit fault-tolerant operation condition to power switch open-circuit fault condition, which was not available earlier. In addition, due to the advantage of rapid diagnosis and no extra hardware cost, the proposed fault diagnosis can improve the fault transient performance and the reliability of the FTPMSM system, which is very suitable for the aerospace application. Further explorations on the multiple power switches open-circuit fault diagnosis approach are also significant and worth pursuing.

References

[1] E. Levi, F. Barrero, and M. J. Duran, "Multiphase machines and drives—Revisited," *IEEE Trans. Ind. Electron.*, vol. 63, no. 1, pp. 429–432, Jan. 2016.

[2] H. Guo, J. Xu, and Y. Chen, "Robust control of fault-tolerant permanent-magnet synchronous motor for aerospace application with guaranteed fault switch process," *IEEE Trans. Ind. Electron.*, vol. 62, no. 12, pp. 7309–7321, Dec. 2015.

[3] N. Bianchi, S. Bolognani, M. D. Pre, and E. Fornasiero, "Post-fault operations of five-phase motor using a full-bridge inverter," in *Proc. IEEE Power Electron. Spec. Conf.*, 2008, pp. 2528–2534.

[4] Y. Sui, P. Zheng, Z. Yin, M. Wang, and C. Wang, "Open-circuit fault-tolerant control of five-phase PM machine based on reconfiguring maximum round magnetomotive force," *IEEE Trans. Ind. Electron.*, vol. 66, no. 1, pp. 48–59, Jan. 2019.

[5] S. Yang, D. Xiang, A. Bryant, P. Mawby, L. Ran, and P. Tavner, "Condition monitoring for device reliability in power electronic converters: A review," *IEEE Trans. Power Electron.*, vol. 25, no. 11, pp. 2734–2752, Nov. 2010.

[6] C. Choi and W. Lee, "Design and evaluation of voltage measurement-based sectoral diagnosis method for inverter open switch faults of permanent magnet synchronous motor drives," *IET Electric Power Appl.*, vol. 6, no. 8, pp. 526–532, Sep. 2012.

[7] I. Jlassi, J. O. Estima, S. Khojet El Khil, N. Mrabet Bellaaj, and A. J. Marques Cardoso, "Multiple open-circuit faults diagnosis in back-to-back converters of PMSG drives for wind turbine systems," *IEEE Trans. Power Electron.*, vol. 30, no. 5, pp. 2689–2702, May 2015.

[8] I. Jlassi, J. O. Estima, S. K. El Khil, N. M. Bellaaj, and A. J. M. Cardoso, "A robust observer-based method for IGBTs and current sensors fault diagnosis in voltage-source inverters of PMSM drives," *IEEE Trans. Ind. Appl.*, vol. 53, no. 3, pp. 2894–2905, May/Jun. 2017.

[9] S. Shao, P. W. Wheeler, J. C. Clare, and A. J. Watson, "Fault detection for modular multilevel converters based on sliding mode observer," *IEEE Trans. Power Electron.*, vol. 28, no. 11, pp. 4867–4872, Nov. 2013.

[10] M. Salehifar, R. Salehi Arashloo, M. Moreno-Eguilaz, V. Sala, and L. Romeral, "Observer-based open transistor fault diagnosis and fault-tolerant control of five-phase permanent magnet motor drive for application in electric vehicles," *IET Power Electron.*, vol. 8, no. 1, pp. 76–87, Jan. 2015.

[11] D. U. Campos-Delgado and D. R. Espinoza-Trejo, "An observer-based diagnosis scheme for single and simultaneous open-switch faults in induction motor drives," *IEEE Trans. Ind. Electron.*, vol. 58, no. 2, pp. 671–679, Feb. 2011.

[12] D. R. Espinoza-Trejo, D. U. Campos-Delgado, G. Bossio, E. Bárcenas, J. E. Hernández-Díez, and L. F. Lugo-Cordero, "Fault diagnosis scheme for open-circuit faults in field-oriented control induction motor drives," *IET Power Electron.*, vol. 6, no. 5, pp. 869–877, May 2013.

[13] K. Debebe, V. Rajagopalan, and T. S. Sankar, "Expert systems for fault diagnosis of VSI fed AC drives," in *Proc. Conf. Rec. IEEE Ind. Appl. Soc. Annu. Meeting*, 1991, pp. 368–373 vol. 1.

[14] H. Yan, Y. Xu, F. Cai, H. Zhang, W. Zhao, and C. Gerada, "PWM-VSI fault diagnosis for a PMSM drive based on the fuzzy logic approach," *IEEE Trans. Power Electron.*, vol. 34, no. 1, pp. 759–768, Jan. 2019.

[15] F. Zidani, D. Diallo, M. E. H. Benbouzid, and R. Nait-Said, "A fuzzy-based approach for the diagnosis of fault modes in a voltage-fed PWM inverter induction motor drive," *IEEE Trans. Ind. Electron.*, vol. 55, no. 2, pp. 586–593, Feb. 2008.

[16] M. A. Masrur, Z. Chen, and Y. Murphey, "Intelligent diagnosis of open and short circuit faults in electric drive inverters for real-time applications," *IET Power Electron.*, vol. 3, no. 2, pp. 279–291, Mar. 2010.

[17] Z. Huang, Z. Wang, X. Yao, and H. Zhang, "Multi-switches fault diagnosis based on small low-frequency data for voltage-source inverters of PMSM drives," *IEEE Trans. Power Electron.*, vol. 34, no. 7, pp. 6845–6857, Jul. 2019.

[18] T. Shi, Y. He, T. Wang, and B. Li, "Open switch fault diagnosis method for PWM voltage source rectifier based on deep learning approach," *IEEE Access*, vol. 7, pp. 66595–66608, 2019.

[19] M. A. Rodríguez-Blanco, A. Vázquez-Pérez, L. Hernández-González, V. Golikov, J. Aguayo-Alquicira, and M. May-Alarcón, "Fault detection for IGBT using adaptive thresholds during the turn-on transient," *IEEE Trans. Ind. Electron.*, vol. 62, no. 3, pp. 1975–1983, Mar. 2015.

[20] M. A. Rodríguez-Blanco *et al.*, "A failure-detection strategy for IGBT based on gate-voltage behavior applied to a motor drive system," *IEEE Trans. Ind. Electron.*, vol. 58, no. 5, pp. 1625–1633, May 2011.

[21] M. Alavi, D. Wang, and M. Luo, "Short-circuit fault diagnosis for three-phase inverters based on voltage-space patterns," *IEEE Trans. Ind. Electron.*, vol. 61, no. 10, pp. 5558–5569, Oct. 2014.

[22] C. Shu, C. Ya-Ting, Y. Tian-Jian, and W. Xun, "A novel diagnostic technique for open-circuited faults of inverters based on output line-to-line voltage model," *IEEE Trans. Ind. Electron.*, vol. 63, no. 7, pp. 4412–4421, Jul. 2016.

[23] B. Lu and S. K. Sharma, "A literature review of IGBT fault diagnostic and protection methods for power inverters," *IEEE Trans. Ind. Appl.*, vol. 45, no. 5, pp. 1770–1777, Sep./Oct. 2009.

[24] C. Cecati, A. O. Di Tommaso, F. Genduso, R. Miceli, and G. Ricco Galluzzo, "Comprehensive modeling and experimental testing of fault detection and management of a nonredundant fault-tolerant VSI," *IEEE Trans. Ind. Electron.*, vol. 62, no. 6, pp. 3945–3954, Jun. 2015.
[25] A. M. S. Mendes, A. J. M. Cardoso, and E. S. Saraiva, "Voltage source inverter fault diagnosis in variable speed AC drives, by Park's vector approach," in *Proc. 17th Int. Conf. Power Electron. Variable Speed Drives*, 1998, pp. 538–543.
[26] A. M. S. Mendes and A. J. Marques Cardoso, "Voltage source inverter fault diagnosis in variable speed AC drives, by the average current Park's vector approach," in *Proc. IEEE Int. Elect. Mach. Drives Conf. Proc.*, 1999, pp. 704–706.
[27] J. A. A. Caseiro, A. M. S. Mendes, and A. J. Marques Cardoso, "Fault diagnosis on a pwm rectifier AC drive system with fault tolerance using the average current Park's Vector approach," in *Proc. IEEE Int. Elect. Mach. Drives Conf.*, 2009, pp. 695–701.
[28] N. M. A. Freire, J. O. Estima, and A. J. Marques Cardoso, "Open-circuit fault diagnosis in PMSG drives for wind turbine applications," *IEEE Trans. Ind. Electron.*, vol. 60, no. 9, pp. 3957–3967, Sep. 2013.
[29] J. O. Estima and A. J. Marques Cardoso, "A new approach for real-time multiple open-circuit fault diagnosis in voltage source inverters," in *Proc. IEEE Energy Convers. Congr. Expo.*, 2010, pp. 4328–4335.
[30] A. M. Santos Mendes, M. B. Abadi, and S. M. A. Cruz, "Fault diagnostic algorithm for three-level neutral point clamped AC motor drives, based on the average current Park's vector," *IET Power Electron.*, vol. 7, no. 5, pp. 1127–1137, May 2014.
[31] H. Yan, Y. Xu, F. Cai, H. Zhang, W. Zhao, and C. Gerada, "PWM-VSI fault diagnosis for a PMSM drive based on the fuzzy logic approach," *IEEE Trans. Power Electron.*, vol. 34, no. 1, pp. 759–768, Jan. 2019.
[32] M. Trabelsi, N. K. Nguyen, and E. Semail, "Real-time switches fault diagnosis based on typical operating characteristics of five-phase permanent-magnetic synchronous machines," *IEEE Trans. Ind. Electron.*, vol. 63, no. 8, pp. 4683–4694, Aug. 2016.
[33] X. Wang, Z. Wang, Z. Xu, M. Cheng, W. Wang, and Y. Hu, "Comprehensive diagnosis and tolerance strategies for electrical faults and sensor faults in dual three-phase PMSM drives," *IEEE Trans. Power Electron.*, vol. 34, no. 7, pp. 6669–6684, Jul. 2019.
[34] J. D. Ede, K. Atallah, J. Wang, and D. Howe, "Effect of optimal torque control on rotor loss of fault-tolerant permanent-magnet brushless machines," *IEEE Trans. Magn.*, vol. 38, no. 5, pp. 3291–3293, Sep. 2002.

Hong Guo received the B.S., M.S., and Ph.D. degrees in electrical engineering from the Harbin Institute of Technology, Heilongjiang, China, in 1988, 1991, and 1994, respectively.

He is currently a Professor with the School of Automation Science and Electrical Engineering, Beihang University, Beijing, China. His research interests include design and control of permanent magnet motor, robust design theory and method of electrical machine, and design theory and method of electrical machine with high reliability.

Si Guo received the B.S. and M.S. degrees in electrical engineering from Beihang University, Beijing, China, in 2011 and 2014, respectively. He is currently working toward the Ph.D. degree in electrical engineering with the School of Automation Science and Electrical Engineering, Beihang University, Beijing, China.

His research interests include fault diagnosis, design, and control of the fault tolerant permanent magnet motor.

Jinquan Xu received the B.S. and Ph.D. degrees in electrical engineering from the School of Automation Science and Electrical Engineering, Beihang University, Beijing, China, in 2009 and 2015, respectively.

From 2012 to 2013, he was a Visiting Scholar with George W. Woodruff School of Mechanical Engineering, Georgia Institute of Technology, Atlanta, GA, USA. He is currently an Associate Professor with the School of Automation Science and Electrical Engineering, Beihang University, Beijing, China. His research interests include fault tolerant permanent magnet motor systems, position sensorless control of fault tolerant motors, fault diagnosis, and robust control.

Xinlei Tian received the B.S. degree in automation specialty from the University of Science and Technology Beijing, Beijing, China, in 2017, and the M.S. degree in electrical engineering from Beihang University, Beijing, China, in 2020. He is currently working toward the Ph.D. degree in electrical engineering with the School of Automation Science and Electrical Engineering, Beihang University, Beijing, China.

His research interests include fault diagnosis and tolerant control of the multiphase permanent magnet synchronous motor.